ANNUAL REVIEWS

Annual Review of Biomedical Engineering

Analytical Techniques for Single-Cell Biochemical Assays of Lipids

Ming Yao, Manibarathi Vaithiyanathan, and Nancy L. Allbritton

Department of Bioengineering, University of Washington, Seattle, Washington, USA; email: yaoming@uw.edu, mvaith@uw.edu, nlallbr@uw.edu

Annu. Rev. Biomed. Eng. 2023. 25:281–309

First published as a Review in Advance on April 17, 2023

The *Annual Review of Biomedical Engineering* is online at bioeng.annualreviews.org

https://doi.org/10.1146/annurev-bioeng-110220-034007

Keywords

single cell, lipids, mass spectrometry, Raman imaging, capillary electrophoresis, thin layer chromatography

Abstract

Lipids are essential cellular components forming membranes, serving as energy reserves, and acting as chemical messengers. Dysfunction in lipid metabolism and signaling is associated with a wide range of diseases including cancer and autoimmunity. Heterogeneity in cell behavior including lipid signaling is increasingly recognized as a driver of disease and drug resistance. This diversity in cellular responses as well as the roles of lipids in health and disease drive the need to quantify lipids within single cells. Single-cell lipid assays are challenging due to the small size of cells (~1 pL) and the large numbers of lipid species present at concentrations spanning orders of magnitude. A growing number of methodologies enable assay of large numbers of lipid analytes, perform high-resolution spatial measurements, or permit highly sensitive lipid assays in single cells. Covered in this review are mass spectrometry, Raman imaging, and fluorescence-based assays including microscopy and microseparations.

Contents

1. INTRODUCTION

Lipids are a diverse group of organic compounds and can be best defined as molecules that are soluble in nonpolar organic solvents but insoluble in water (1). They can be hydrophobic (typically nonpolar) or amphiphilic (a hydrophilic head group at one end and a hydrophobic region at another). For example, phospholipids (PLs) possess one or more phosphate groups in addition to long acyl chains enabling these molecules to align as a bilayer (or two mated monolayers) and form cellular membranes, with the hydrophobic acyl chains facing each other and the hydrophilic phosphate-bearing regions facing the aqueous environment. This bilayer membrane then acts as a barrier surrounding the intracellular constituents and creating a barrier to the extracellular environment. Lipids also provide a multitude of essential biological functions, for example, acting as signaling molecules, providing energy storage, localizing interacting proteins, and generating bioactive metabolites. Lipids in eukaryotic cells can be classified in many ways, with eight categories developed by the International Lipid Classification and Nomenclature Committee being the most commonly used (2). These lipid categories are fatty acyls, glycerolipids (GLs), glycerophospholipids (GPLs), sphingolipids (SLs), saccharolipids, polyketides, sterol lipids, and prenol lipids. Fatty acyls include fatty acids (FAs), fatty alcohols, aldehydes, and esters and often act as building blocks for complex lipids such as eicosanoids, which act to regulate inflammation. Cellular and organelle membranes are formed from GLs and GPLs. However, some members of these lipid groups such as GLs and free fatty acids (FFAs) act as signaling molecules to regulate energy homeostasis, insulin secretion, gene expression, cell survival, and cell proliferation (3). Members of the SL family such as ceramide, sphingosine, and their metabolites play a role in signal transduction pathways, while other SL members direct protein sorting, mediate cell-to-cell interactions, or form signaling hubs (lipid microdomains and rafts) (4). Members of the remaining four lipid categories (saccharolipids, polyketides, sterol lipids, and prenol lipids) play diverse roles including participation in lipid bilayers, biosynthetic pathways, and signaling pathways, as well as antioxidant functions (1). Considering these varied roles of lipid categories, cellular health and function clearly are greatly dependent on lipid metabolism and lipid environment.

LD: lipid droplet

Not surprisingly, cellular lipid metabolism is a complex network with an interplay of the various members of the lipid classes, the participation of large numbers of enzymes, and locations throughout a eukaryotic cell [organelles, membranes, and lipid droplets (LDs)]. Alterations in this

interconnected network can lead to significant consequences for the cell, organ, and/or organism. Dysfunction in lipid metabolism and handling is associated with many diseases, including cancer, cardiovascular disease, diabetes, autoimmunity, and neurodegeneration (5–9). Cancer cells particularly are adept at highjacking lipogenic and lipolytic pathways to support their proliferation and survival (10). For example, both breast and pancreatic cancer cells alter triacylglycerol FA levels by enhancing the activity of acid synthase, which is a key lipogenic enzyme in cancer pathogenesis and a well-known cross-talk node in several cancer-related networks (11). Several inflammatory and autoimmune diseases such as systemic lupus erythematosus, atherosclerosis, fatty liver disease, and cardio-metabolic disease are associated with impaired lipid metabolism of FFAs, triglycerides (TGs), lipopolysaccharides, and cholesterol esters (12, 13). In all of these diseases, the behaviors of single cells and/or their clonal progeny have profound impact on disease progression and outcome. Understanding the cellular and molecular mechanisms at single-cell resolution using multi- or transomics approaches reveals information on cellular heterogeneity and progression of disease pathogenesis. This cell-to-cell heterogeneity extends to the information flow through lipid signaling and metabolic pathways. For example, accumulation of FAs is correlated with the initiation of pancreatic ductal adenocarcinoma, and intracellular heterogeneity in FA distribution results is associated with metastasis, which has a 5-year survival rate of only 9% (14). Similarly, in metabolomic diseases, heterogeneous thermogenic capacity of a subpopulation of mature adipocytes, called beige adipocytes, can result in obesity and diabetes (15). Thus, understanding lipid handling at the single-cell level is critical to revealing intracellular as well as intercellular heterogeneity and the impacts to human health and disease processes.

TLC: thin-layer chromatography

MS: mass spectrometry

Lipids are more challenging to assay than other cellular constituents such as ribonucleotides and proteins primarily due to their lack of repeating residues, high molecular complexity, hydrophobicity, tendency to aggregate, and propensity to bind to surfaces. Nevertheless, a number of analytical methodologies such as thin-layer chromatography (TLC), high-performance liquid chromatography (HPLC), gas chromatography, and mass spectrometry (MS) have been successfully applied to build the field of lipidomics, providing insights into the diversity of lipid species in humans and their roles as building blocks, signaling agents, structural supports, energy storehouses, and temperature regulators. Importantly, enzymes within many lipid synthetic or metabolic pathways, for example, phosphoinositide 3-kinase and sphingosine kinase (SK), have become pharmaceutical targets with a goal of modulating disease pathways and further driving the need to understand these important molecules (16). The vast majority of experimental work related to lipid pathways has been performed on bulk tissue specimens or pooled cell lysates due to the ease in extracting intracellular products to provide a large sample size. Only recently have analytical methods achieved the sensitivity and specificity need to assay lipids from a single mammalian cell of picoliter volume. One ongoing analytical challenge is the wide range of lipid analyte concentrations within a cell; for example, plasma membranes are enriched in cholesterol, phosphatidylserine, and sphingolipids, while the endoplasmic reticulum is deprived of these lipids. In addition to this heterogeneous lipid distribution between membranes, the distribution of lipids varies across the membrane bilayer. This aspect demands high dynamic range, excellent sensitivity, and spatial resolution from an analytical assay, which in practice means that most analytical methods target a subset of cellular lipids. Lipids are also found in a range of cellular subcompartments and in varying states, for example, insoluble aggregates, membrane incorporated, and protein bound, making some lipids readily accessible for analytical assays while other lipids have yet to be assayed from single cells. Innovations in a number of analytical tools (MS, microscopy, Raman spectroscopy, chromatography, electrophoresis, and fluorescent probes) now enable a plethora of lipids to be quantified from single cells; however, lipidome characterization in these ultrasmall

samples remains far from mature. This review focus on recent developments in single-cell lipid assays including the method's working principles, advantages, limitations, and applications.

MALDI-MS: matrix-assisted laser desorption/ionization mass spectrometry

SI-MS: secondary-ion mass spectrometry

ESI-MS: electrospray ionization mass spectrometry

2. MASS SPECTROMETRY OF LIPID ANALYSIS IN SINGLE CELLS

Because MS possesses high sensitivity and specificity and does not require labels or probes to detect analytes, it has been widely exploited for single-cell analysis, including the assay of lipids. MS offers a nontargeted assay approach to identify unknown lipids, and assays do not need to focus on a preidentified lipid species. Single-cell mass spectrometry (SCMS) can be performed using different desorption/ionization techniques and sampling environments, adding to the versatility of MS. Desorption/ionization strategies include matrix-assisted laser desorption/ionization mass spectrometry (MALDI-MS), secondary-ion mass spectrometry (SI-MS), and electrospray ionization mass spectrometry (ESI-MS) (17). Methods requiring that the sample be placed under a vacuum (MALDI-MS and SI-MS) are highly sensitive, with a 50-attomol limit of detection and high spatial resolution of sub-50 μm, but do require sample processing (fixation and dehydration) and may suffer from unwanted spatial distortions or chemical reactions. In contrast, ESI-MS is performed on cells in an ambient environment with minimal sample preparation (18–20). The cellular contents can be introduced directly into the mass spectrometer or using a transfer device such as a capillary. More recently, laser microbeams have been used to dissect single cells to provide spatial resolution, albeit at a reduced sensitivity (21, 22). MALDI imaging mass spectrometry (MALDI-IMS) is increasingly popular, displaying a subcellular spatial resolution of 25–50 μm^2 pixel size (23). Comprehensive reviews on SCMS are available, although they are focused largely on protein-based assays (24). This section highlights the latest SCMS techniques in lipidomics as well as their advantages, limitations, and opportunities (**Figure 1**).

2.1. Matrix-Assisted Laser Desorption/Ionization Mass Spectrometry

Laser desorption/ionization MS techniques for single-cell lipid measurements have evolved greatly in recent years, particularly with the development of MALDI-MS for whole cell and subcellular lipid assays (23, 25). In MALDI-MS, a sample precoated with an energy-absorbing matrix is irradiated by a laser beam, and energy absorbed by the matrix is then transferred to the sample, facilitating sample desorption and ionization (**Figure 1*a***). Ionized sample constituents enter the mass spectrometer, followed by measurement of their mass-to-charge (m/z) ratios. The matrix choice typically depends on the analytes to be assayed so as to optimize energy transfer, and a variety of different matrices have been employed successfully for lipid measurements by MALDI-MS including α-cyano-4-hydroxy cinnamic acid, 2,5-dihydroxybenzoic acid, and 9-aminoacridine (26).

The MALDI process is typically coupled to a time-of-flight (TOF) mass spectrometer providing access to a wide ion mass range (m/z) from as low as 100 Da to more than 500 kDa but with a lower linear mass resolution of only >5,000 FWHM. An asset of MALDI is the ability to couple to other MS detectors, for example, tandem MS (MS/MS) for structural characterization or Fourier-transform ion cyclotron resonance mass spectrometry (FTICR-MS) for high-precision measurements enhancing MALDI capabilities and applications in single-cell lipidomics. However, initial applications of MALDI-MS for lipid-based assays were low in spatial resolution, sampling the entirety of a cell, and often applied to a large cell type such as an oocyte (27). A wide range of lipids including sphingomyelins (SMs), phosphatidylcholines (PCs), and TGs were quantifiable, revealing important insights into membrane lipid compositions under various environmental conditions and at various developmental stages of an embryo. Although these measurements provided significant advancements in knowledge, a challenge was that only the most abundant lipids were

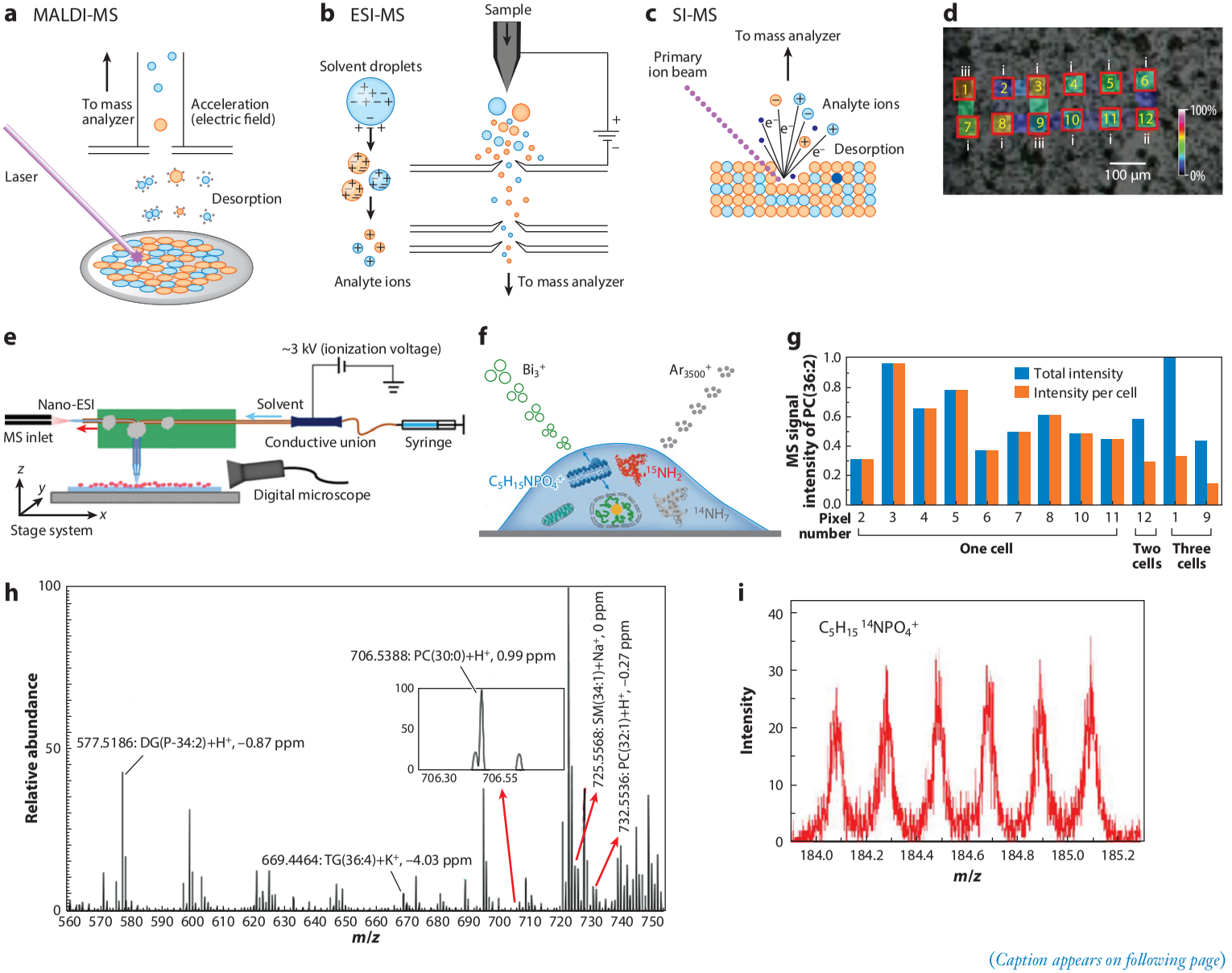

(*Caption appears on following page*)

Figure 1 (*Figure appears on preceding page*)

Mass spectrometry assay of lipids in single cells. Schematics describe the working principles of (*a*) matrix-assisted laser desorption/ionization mass spectrometry (MALDI-MS), (*b*) electrospray ionization mass spectrometry (ESI-MS), and (*c*) secondary-ion mass spectrometry (SI-MS). (*d*) A549 cells combined with a 9-aminoacridine matrix were examined by MALDI imaging mass spectrometry. Pixels positive for PC(36:2) are marked with yellow numbers, and the cell count in every pixel is marked with white Roman numerals in the microscopy image. (*e*) The schematic demonstrates the use of a single-probe ESI to assay for phosphatidylcholines (PCs), sphingomyelins (SMs), diglycerides (DGs), and triglycerides (TGs) in single HeLa cells. (*f*) The schematic shows the assay of a single cell by SI-MS. A Bi_3^+ liquid metal ion gun was used to scan across the cell to acquire an XY image, while Ar_{3500}^+ was used to obtain depth or Z profiles. (*g*) The total and average MS signal intensities for PC(36:2) from the extracted pixels in panel *d* are shown. (*h*) Displayed are the mass spectrometry data obtained in a mass range from *m/z* 560 to *m/z* 750 for the experiment shown in panel *e*. (*i*) Data are shown demonstrating the fragment ions obtained from SM ($C_5H_{15}{}^{14}NPO_4^+$) when a cell was imaged at submicrometer resolution by time-of-flight SI-MS, as depicted in panel *f*. Panels *d* and *g* adapted with permission from Reference 33. Panels *e* and *h* adapted with permission from Reference 39; copyright 2014 American Chemical Society. Panels *f* and *i* adapted with permission from Reference 57; copyright 2017 Elsevier.

detectable, with many rare species (important in cell signaling) undetectable due to their low abundance; for example, even with an attomole detection limit, only the most abundant lipid species are detectable (28). These applications, however, pointed the way for improved instrumentation and methods to enhance spatial resolution, throughput, and sensitivity.

Improved sample preparation protocols, laser illumination strategies, and image processing and reconstruction methods have enabled significant increases in spatial resolution, throughput, and multicomponent analysis. Cell lyophilization applied to large cell types such as neuronal ganglion cells opened the door to subcellular sampling of cells with assay of membrane phospholipids such as PCs, which could be detected with different profiles in a neurite versus a neuronal cell body (29). While results from this work provided preliminary understanding of neuronal lipid metabolism, the large laser spots used for MALDI-MS still yielded poor sensitivity and spatial resolution. The use of overlapping laser spots to oversample as well as complete sample ablation at each laser beam location enabled resolutions greater than that of the microbeam diameter but created tissue distortions such as analyte delocalization, ultimately limiting this strategy. Improvements in both sensitivity and spatial resolution were achieved by positioning the laser behind the sample and irradiating from the sample backside (30). This geometry reduced the working distance between the sample and optics, enabling a submicron laser beam spot on the sample and a submicron to micron spatial resolution during imaging. In this proof-of-concept work, the distribution of intact lipids at a single *m/z* 782 was imaged in cultured human embryonic kidney and colon cancer cells. Spatial resolution and sensitivity also have been enhanced by optimizing sample preparation, measurement parameters, and computational image reconstruction combined with more traditional instrumentation to image a range of lipids [PCs, SMs, diglycerides, phosphatidylethanolamines (PEs), phosphatidylinositols, and/or TGs] at cell-sized resolution (5–10 μm) (23, 31).

Three-dimensional MALDI-IMS has also been developed by stacking and reconstructing traditional 2D MS images into 3D images (25). A variety of strategies have been developed to enhance the rate of lipid analysis in single cells to enable large numbers of cells to be assayed. The use of a laser for sample desorption/ionization provides a speed advantage due to both the ability to rapidly scan the beam and the very short pulse durations (<1.1 ns). Placing cells into microwell arrays to preposition cells at known locations resulted in 40% single-cell capture efficiency, which when followed by MALDI-IMS enabled the assay of 12 lipid species in single cells by extracting relative signal intensity data from every pixel in the images over several minutes (32, 33). Integration of cell-recognition software with automated instrumentation permitted cells randomly located on a slide to be sequentially examined by MALDI-MS with assay of up to 30,000 cells (34). A feature of MALDI-IMS is the ability to combine MS with other analytical methods, for example, optical microscopy (fluorescence or bright-field), to create information-rich data sets

as well as to coregister the MALDI-MS data with known histologic structures (35). While these methods have improved spatial resolution and analytical throughput, the performance of MALDI-IMS remains focused on high-abundance lipid species, particularly when combined with TOF or quadrupole-based detection ($\leq$12 lipid species or features).

One reason for the limitation of MALDI-IMS to high-abundance lipids in single cells is the low mass resolution of the TOF detectors, which ensures that low-abundance species are overshadowed by all of the highly abundant lipids. FTICR-MS offers both high mass resolution and high mass accuracy, enabling the detection of larger numbers of lipid species compared with those from other MS detectors. When combined with MALDI, these assets are retained along with the MALDI advantage of high single-cell analysis rates; for example, heterogeneous liposaccharide distributions were measured in >100 RAW 264.7 cells on a timescale of hours using FTICR-MS (36). Up to 670 ions in the lipid mass range could be detected in large numbers of single cells with excellent throughput (100s of cells/h) (34–37). As another example, up to 500 lipid features were detected within 30,000 rodent brain cells, from which 101 significantly distinct cell clusters could be correlated with neuronal or astrocytic lipid markers. Due to the high mass resolution, impressive chemical details were possible, with the most common lipids identified as $[PC(32:0)+H]^+$ and $[PC(34:1)+H]^+$ in 98.9% and 89.5% of cells, and with $[PC(34:1)+K]^+$ and $[PG(40:2(OH))+Na]^+$ present in <1% of cells (34). To achieve the needed sensitivity, spatial resolution was limited to the size of a cell or larger (25–100 μm) in these studies. A challenge was the need to use reference data banks for lipid identification, since tandem MS is not possible on these small-scale samples. However, the ongoing construction of high-quality lipid databases will address this drawback in the future. Finally, the high cost of FTICR-MS will likely limit this technology to core facilities and centers at large institutions.

2.2. Electrospray Ionization Mass Spectrometry

ESI-MS is a low-energy ionization method that yields minimal fragmentation of analytes. In ESI, charged droplets of analyte solution are produced at the outlet of a capillary tip and are accelerated under an electric field toward the MS detector (**Figure 1*b***). Application of a drying gas or heat progressively evaporates the solvent into charged ions, allowing the analyte to enter the gas phase prior to the MS inlet. ESI possesses high ionization efficiency and is readily coupled to chromatographic devices for sample separation prior to MS analysis, but it does yield more complex spectra than MALDI with multiply charged species (38). Sufficient volume and quantity of sample is required to accommodate sample loss in the chromatographic step, making assay of single-cell contents challenging. The complex makeup of biologic samples can lead to matrix effects or ion suppression, reducing the accuracy and precision of the MS analysis. Finally, ESI-MS is challenging to integrate with other cellular analysis methods such as microscopy. A plethora of technologies have been developed in recent years to overcome these challenges including nano-ESI, desorption ESI (DESI), laser ablation ESI, probe ESI, and capillary ESI (39–43). We cover a subset of ESI-MS techniques in this section: Perhaps the most applicable strategy to single-cell lipid assays is nano-ESI, a derivative of ESI tailored to accommodate small volume samples with limited analyte concentrations.

Nano-ESI uses an emitter tip with a typical internal diameter of approximately 1 μm, employs low solvent flow rates of 20 to 40 nL min^{-1} (compared with ESI's typical rate of 100 μL min^{-1}), involves reduced sample consumption and improved detection sensitivity, does not require a drying gas or heating, and applies a high voltage of 1–2 keV for ionization to form an electrospray. A chromatographic step is not required as a first stage for nano-ESI, so samples can be directly injected into the MS detector (eliminating sample loss on a separation column). The dilute sample

(~0.5 to 5 pmol/mL) also minimizes matrix effects. Together, these features provide a high ionization efficiency and high signal-to-noise ratio relative to that of standard ESI. A convenient aspect is that the nanotip (most often a pulled capillary) can serve as both a collection device for the cell contents as well as the nano-ESI tip. Precision spatial movement of the nanotip by a micromanipulator is required to precisely collect the cell or its contents. Nano-ESI can be mated with other analytical methods, for example, microscopy and patch clamp. A significant advantage of nano-ESI is the ability to sample and analyze single cells from within intact tissue slices or organs, providing a more physiologic output than that obtained from disaggregated, isolated cells (44). A variety of capillaries, probes, patch-clamp pipettes, and microfluidic devices under manual or automated operation have been used to collect single cells or their contents as well as to function as the nano-ESI tip (39, 44–48). When a chromatographic step is not coupled to nano-ESI, a lipid extraction step is often incorporated to enhance lipid introduction into the nano-ESI instrument. Many extraction strategies have been employed successfully including preaddition of solvent around the cell just prior to cell sampling, inline addition of solvent as the cell or cell lysate flows toward the emitter tip (46, 49), use of a dual-barrel capillary to introduce solvent through one barrel as a cell is loaded into the other barrel, and other strategies (39, 50). Cell lysis (and lipid solubilization) during whole-cell collection is accomplished by using the sampling tip and lipid extraction solvent, by incorporating ultrasonic lysis (45), or by addition of inline filters with cell-puncturing spikes (zinc oxide nanothorns) (46). Nano-DESI takes this step to the next level by using a second solvent-carrying capillary for lipid extraction, forming a liquid bridge connecting to the emitter capillary (51). An alternative version, IR-MALDESI, is, as the name implies, a hybrid of MALDI and ESI using an infrared laser to ablate biological samples, followed by ESI (52).

Nano-ESI and its various forms are also compatible with subcellular sampling, depending on the exact sampling strategy, with a resolution of ~10–100 μm (47, 49). Cytoplasmic sample collection using a patch-clamp pipette could, in theory, leave a cell alive after sampling and viable for other assays (although sensitivity will be a challenge) (47). Throughput has been enhanced (520 lipid features from 30,000 cells and 38 cells/min) by automated movement and positioning of the cell-collection tip, extraction steps, and incorporation of label-free flow cytometry and microfluidics for cell queuing into the emitter tip (20, 53, 54). Nano-ESI has been applied to detect lipids in a wide range of mammalian cells (HeLa cervical cells, liver cells, white blood cells, breast cells, neuronal cells, and others) (39, 44–48) and subcellular components (LDs) (49); however, the majority of lipid analytes detected in cells have been the abundant species such as PCs, PLs, PEs, and phosphatidic acids (PAs). Despite the theoretical advantages of direct injection methods, utilizing a pre-ESI separation step has yielded very high performance. Coupling nanoflow liquid chromatography with nano-ESI enabled detection of 236 lipids from four lipid classes (SLs, sterol lipids, GLs, and GPLs) in healthy and diseased mammalian hippocampal slices, providing an improved understanding of lipid homeostasis in brain disease (47). Others have used a bulk preseparation step, selectively isolating PLs by incubating a single-cell lysate with TiO_2-coated Fe_3O_4 nanoparticles followed by elution from the beads and assay by nano-ESI (55). This strategy permitted detection of 18 different PLs with limits of detection of ~0.01 μg/L in the MS/MS spectra.

2.3. Secondary-Ion Mass Spectrometry

Traditional SI-MS employs a high-energy primary ion beam (Ar^+, O^{2+}, N^{2+}, and others) to bombard the sample surface, releasing charged secondary ions that are then directed into an MS detector (56) (**Figure 1*c***). Like MALDI, SI-MS is performed under a vacuum, requiring samples to undergo chemical or high-pressure/freezing fixation prior to analysis. Since the ion beam can be focused to a tight spot (and is not diffraction limited) the spatial resolution is exceptional at

a sub-50-μm range with a depth of approximately 20 μm (57). While the ion beam efficiently lifts off sample, providing excellent sensitivity, the high-energy beam also fragments sample molecules into a size range of hundreds of daltons, making data interpretation more challenging than low-energy ionization methods such as MALDI and ESI. However, since the ion beam removes the top layer of sample, 3D imaging is possible by sequential XY scanning. To improve SI-MS compatibility with single-cell lipid imaging, recent work has focused on several technological innovations: application of low-energy cluster-ion beams with or without an energy-absorbing matrix, optimization of fixation strategies, and enhancement of 3D imaging methods using sample labeling methods. The recent development of cluster ions as the primary beam in SI-MS enables sample surface sputtering at low energy with less sample damage and release of higher molecular weight sample molecules including intact lipid molecules (57, 58). For example, C_{60}^+ SI-MS has been applied to image cells and assay lipid composition of the plasma membrane followed by assay of lipids within the cytosol of the same single cell (59). Using Au_3^{2+} as the cluster ion, breast cancer stem cells were demonstrated to have different FA content than non-stem cells (60). Enhanced and validated preservation strategies including plunge freezing in ethane to eliminate sample fracture and characterization of glutaraldehyde-based fixation and the impact on lipids have also advanced single-cell lipid assays by tandem SI-MS (61). Ionic liquids have been applied to samples to perform matrix-enhanced SI-MS, enhancing the sputtering/ionization efficiency and chemical signals attainable from single cells with quantification of PC lipids in neuronal cells (62).

Powerful variants of SI-MS such as multi-isotope imaging MS (MI-MS) use stable isotope labeling of cells and a scanning ion beam to quantitatively image the distribution within cells of a stable isotope such as ^{13}C. These advances enabled a better understanding of the mechanism of long-chain FFA transport across an adipocyte's cell membrane (28). Using MI-MS, the localization of intact lipid species such as PCs across the surface of single neurons as well as colocalization with vitamin E and cholesterol was assessed (28). Another innovative variant of SI-MS is nano-SI-MS, which uses a high-energy focused beam to achieve a spatial resolution down to ~50 μm and is suitable for detecting small (mainly monoatomic and diatomic) ions (63).

3. RAMAN-BASED TECHNOLOGIES

When light impinges upon a molecule, the light can be scattered elastically, that is, without a change in energy (Rayleigh scattering), or inelastically, that is, with a change in energy (Raman scattering) (64–66). In Raman scattering, the energy from the photon initiates a vibrational change in the molecule and a subsequent scattered photon, which can be lower in energy (Stokes scattering) or higher in energy (anti-Stokes scattering) than the incident radiation. The energy difference is characteristic of the excited chemical bond, leading to insights into the molecular species illuminated (64, 67, 68). Due to the high concentration and/or strong scattering from a number of bonds (e.g., C–H, C–C, C=C) commonly found in organic molecules, Raman scattering has emerged as a powerful tool for cellular imaging (64, 65, 69). Each chemical bond possesses a characteristic vibrational mode or Raman shift; for example, the C–H wave number lies in the region of 2700–3100 cm^{-1}, while C–H_2 is in the 1400–1500 cm^{-1} range, C–C is in the 600–1300 cm^{-1} range, and C=C is in the 1640–1680 cm^{-1} range (70). Because Raman scattering is based on a vibrational resonance, Raman-based imaging is not affected by photobleaching nor sensitive to the surrounding environment (as in the case of fluorescence). The infrared wavelengths typically used for cellular Raman imaging confer high sample penetrance with reduced photodamage. In particular, Raman scattering has been used to image a wide range of molecules in cells such as lipids, proteins, and DNA. Raman spectra can be acquired within seconds, especially with the newer Raman methods, due to the high total concentration of biological molecules in cells. Lipids in particular, with

SRS: stimulated Raman scattering

CARS: coherent anti-Stokes Raman scattering

their large number of CH_2 groups, are well suited for Raman imaging (64, 65, 69, 70) and can be assessed in living or fixed single cells with high contrast and high resolution in a label-free and nondestructive manner (68). However, a challenge for all Raman-based methods in imaging biological samples is the complex mixture of molecules present with similar vibrational modes, making the identification of specific molecular species quite challenging and the detection of low concentration species impossible. Nevertheless, Raman microscopy has emerged as a powerful tool for biological imaging to advance our understanding of the mechanisms behind physiological and diseased states.

Raman imaging of lipids within single cells typically employs either spontaneous Raman scattering, stimulated Raman scattering (SRS), or coherent anti-Stokes Raman scattering (CARS), although other strategies are possible (64, 65). With spontaneous Raman-based microscopy, a single laser beam illuminates the biological sample, exciting molecules to a higher vibrational state, followed by light emission at a longer wavelength (**Figure 2*a***). Due to the very small scattering cross section ($\sim 10^{-30}$ cm^2 sr^{-1}) for spontaneous Raman scattering, light emission is weak ($\sim 1/10^{16}$ that of fluorescence), resulting in long imaging times (many minutes/image) with use of high-laser powers even for high concentration analytes such as cellular lipids. The high required illumination intensities also yield significant background in the form of sample autofluorescence and Raleigh scattering. SRS and CARS address many of these challenges, providing stronger signals with lower

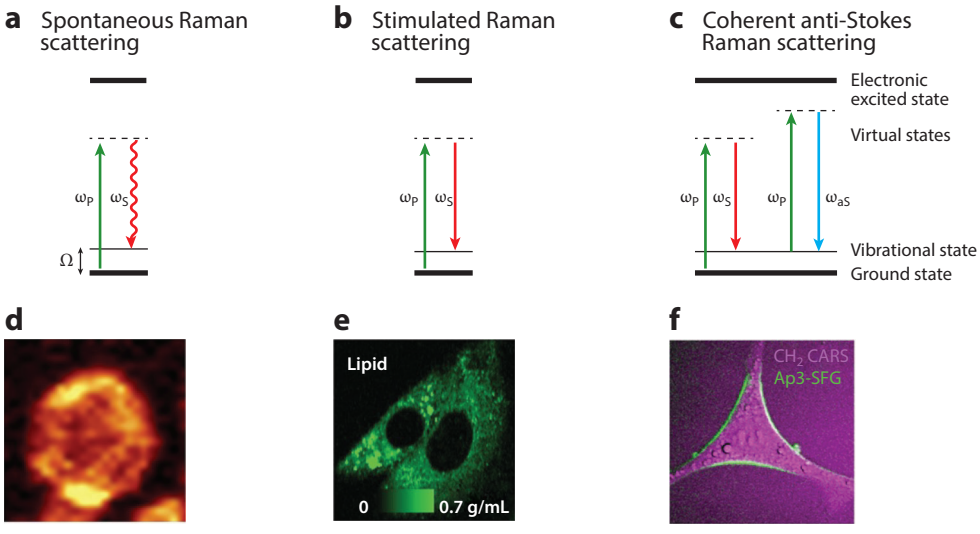

Figure 2

Raman imaging of single cells. (*a–c*) Schematics demonstrating the energy level diagrams in Raman imaging. (*a*) Spontaneous Raman scattering. The straight line (*green*) indicates the pump beam at ω_P, and the curved line (*red*) denotes the scattered light at a longer wavelength ω_S. (*b*) Stimulated Raman scattering (SRS). Two lasers, a pump (ω_P) and a Stokes beam (ω_S), impinge upon a sample, with stimulated emission occurring when $\Delta\omega(\Delta\omega = \omega_P - \omega_S)$ equals a molecular vibration frequency. (*c*) Coherent anti-Stokes Raman scattering (CARS). In CARS, a pump (ω_P) and a Stokes beam (ω_S) illuminate the sample, and when $\omega_P - \omega_S$ matches the molecular vibration frequency, an anti-Stokes signal at $2\omega_P - \omega_S = \omega_{aS}$ is generated. (*d*) Distribution of lipids (1420–1460 cm^{-1}) in a pulmonary cell obtained by spontaneous Raman imaging. (*e*) An SRS image showing the concentration of cytoplasmic membrane lipids in live melanoma cells. (*f*) A CARS image of a neuronal cell. The purple color shows CH_2 bonds, while the green color is the plasma membrane dye, Ap3-SFG. Panels *a–c* adapted with permission from Reference 65. Panel *d* adapted with permission from Reference 95. Panel *e* adapted from Reference 123 (CC BY-NC-ND 4.0). Panel *f* adapted with permission from Reference 136; copyright 2020 American Chemical Society.

background noise. For SRS, two laser beams (pump and Stokes beams) are incident on the sample. When the frequency difference between the two beams matches a molecular vibration, stimulated excitation of the vibrational transition occurs with an intensity loss at the scattered pump wavelength and an intensity gain at the scattered Stokes wavelength (**Figure 2*b***). Measurement of this energy gain/loss can then be accomplished, albeit with sophisticated equipment. An advantage of SRS is the proportionality of the signal to molecular concentration and the spectral match to spontaneous Raman scattering. CARS, which can be accomplished using a multitude of strategies, also employs two beams (pump and Stokes), but in this instance, molecules are stimulated while in their vibrational state, yielding a higher-energy emission (anti-Stokes shifted) (67, 71) (**Figure 2*c***). CARS provides fast, high-sensitivity measurements due to emission at a shorter wavelength (with facile spectral separation from longer-wavelength sample autofluorescence). CARS, however, requires high-intensity beams, which can lead to multiphoton absorption and material damage. The required complex instrumentation also requires careful beam synchronization. A number of compound microscopes that combine Raman imaging with traditional optical microscopes have demonstrated added value to that of Raman imaging alone (72–78). These compound microscopes incorporate Raman imaging with bright-field, fluorescence, or confocal microscopy to provide simultaneous information on lipids and other cellular constituents such as proteins, including their relative spatial locations (75, 79–84). As an example, SRS combined with confocal fluorescence microscopy enabled high-speed multicolor imaging, providing insights into LD biology and other markers associated with these LDs at the single-cell and even the subcellular level (79, 81–83). All Raman imaging methods now can be configured to read out continuous spectra, for example, hyperspectral Raman images, enabling a greater characterization of the complex lipid mixtures within cells (85–89). Comprehensive reviews with a sole focus on Raman microscopy are available, and this section highlights spontaneous Raman scattering, SRS, and CARS with a focus on their advantages, limitations, and opportunities in the measurement of lipids in single cells (84, 90, 91) (**Figure 2**).

3.1. Spontaneous Raman Imaging

Spontaneous Raman spectroscopy has enabled lipid assays in single cells and has many advantages relative to the newer Raman imaging methods, including simpler instrumentation with a single laser that is readily focused to submicron spot sizes easily scanned across a sample. This approach enables a typical imaging spatial resolution in the range of ~0.3–0.6 μm (92, 93). A strength of Raman spectroscopy in lipid analysis is the ability to assess the degree of lipid unsaturation as well as the ratio of *cis*/*trans* isomers in lipid samples (94). The emission spectral resolution is typically in the range of ~1.5–3 cm^{-1} (92, 95–97). The collection of spectra at each image pixel provides high-value chemical information but can require up to 1 s/pixel, yielding long times to image entire samples (92, 98–100). The availability of commercial microscopes (WITec and Renishaw, for example) that combine spontaneous Raman scattering and confocal microscopy also make the technology accessible to nonexperts. Due to the inherently weak signal of spontaneous Raman scattering and the complex nature of cellular structures, the method generally focuses on organelles with high lipid concentration such as LDs or incorporates Raman labels such as deuterated- or alkyne-labeled compounds to enhance analyte detectability.

The combination of spontaneous Raman scattering with other microscopy methods such as confocal or atomic force microscopy, and even other Raman techniques, has emerged as a critical enabler to measure lipids within LDs and other subcellular organelles (72–78, 80, 101–103). A number of studies have combined Raman and fluorescence microscopy with fluorescent lipid probes such as Nile Red, Oil Red O, ReZolve-L1™, or BODIPY 493/503 with Raman imaging to label lipids, especially LDs, directly enhancing sensitivity, lipid characterization, and spatial

precision (98, 104, 105). Another example of the advantages of compound microscopes is the spatial targeting of Raman measurements to fluorescently labeled organelles (mitochondria or endoplasmic reticulum) for fast, efficient, subcellular measurements as opposed to the time-consuming imaging of an entire cell (80). This approach, termed micro-Raman assay, has enabled assay of the lipid unsaturation, *cis/trans* isomer ratio, sphingolipids, and cholesterol levels in live cells. Another compound system has been demonstrated to acquire Raman hyperspectral images with a 4-min temporal resolution followed by comparison of the Raman data with that of quantitative phase microscopy to distinguish living cell types (72).

Cellular constituents have little Raman scattering between 1800 and 2800 cm^{-1}, also known as the silent region. Raman tags with spectra in this region have been developed to track intracellular molecules without interference from the Raman signal of the endogenous cellular components (104, 106–108). Commonly used tags such as alkynes, nitrile, and deuterium provide a strong Raman scattering peak in the silent region and have facilitated identification of organelles or specific molecules within the complex cellular environment (104). A series of alkyne-tagged coenzyme Q analogs labeling the mitochondria permitted visualization of the spatial location of this Raman tag (109). An alkyne-tagged cholesterol labeled LDs in a liver cancer cell line, yielding the molecular identification of as many as seven different constituents of LDs, as well as the spectral isolation of three structurally different lipid species (110). Falcarinol, an anti-inflammatory polyacetylene that naturally scatters in the silent region, has been used to investigate cellular changes resulting from induced endothelial dysfunction (111). Deuterium is also commonly used as a Raman tag to visualize lipids (112, 113). Advances in the understanding of lipid physiology created through the use of deuterium tags include the visualization of lipid translocation between endocytic vesicles and LDs in macrophages (114), intracellular lipid metabolism in macrophages (113), time-dependent investigation of FA distribution in macrophages (115), and the quantification of stearic acid uptake and accumulation in LDs of cat oocytes (116). One recent innovation incorporated H-alkyne and D-alkyne labels into long-chain FA probes to distinguish between two structurally similar small molecules in living cells (117).

3.2. Stimulated Raman Scattering Imaging

SRS is a nonlinear optical process for which the scattered signal is generated at the focal plane of the sample, enabling intrinsic 3D sectioning by scanning in the x, y, and z axes with submicron to micron spatial resolution (65, 70). SRS is characterized by a low background (orders of magnitude lower than spontaneous Raman scattering), because a nonresonant signal is not present; that is, when the frequency difference between the pump and Stokes beams does not match a vibrational transition, then no energy exchange occurs between the scattered signals. This translates into detection limits of greater than ~0.1 mM (often tens of mM) depending on the molecule. High-speed imaging of entire samples (ms/pixel) is possible, especially when measuring at a single wave number. Since an intensity difference is the measured signal riding on the pump and probe Raman-scattered photons, optical modulation (>2 MHz) and phase-sensitive detection are needed to differentiate the scattered signal from the incoming excitation beams. This requires sophisticated instrumentation (in addition to the lasers), such as a lock-in amplifier to detect the stimulated Raman loss or gain, but does enable the measured signal to be of high intensity relative to that measured for spontaneous Raman scattering or CARS (65, 70). Although low in magnitude relative to other Raman methods, SRS does have a background that is of complex origin and thus is challenging to mitigate; however, frequency modulation of the incident light can be employed to minimize this background (118). Other innovations such as hyperspectral SRS enable imaging over a range of wave numbers (300 cm^{-1}) at each pixel to obtain detailed spectral information. The collection of Raman spectra permits deconvolution of overlapping

Raman signals due to the presence of multiple molecules. This analysis is particularly useful in reconstructing lipid types in an imaged sample (85, 119, 120). Moreover, hyperspectral imaging in combination with broadband imaging offers an imaging range as great as 600 cm^{-1} with a fast speed of ~8 μs/pixel (85). A major application of SRS lipid imaging in single cells has focused on LDs and other high-concentration lipids due to the poor sensitivity relative to other methods, for example, mass spectrometry or fluorescence microscopy (121–124).

Exciting advances are underway in SRS imaging of single cells. For example, customized equipment paired with new computational tools enables the measurement of protein mass, lipid mass, and water content in the same single cell with 3D resolution, permitting internal comparison of concentrations (123). This system provided a sensitivity of ~0.015 g/mL and a spatial resolution of 1.18 and 1.90 μm in the lateral and axial dimensions, respectively. Hyperspectral SRS imaging has been used to identify lipid content differences in cancerous cells versus normal cells to understand fundamental differences in the lipid biology of these cells (81, 119, 120). Even LDs within the two types of cells were observed to have distinct lipid signatures (120). A growing trend is the integration of SRS with other types of imaging methods, for implementing either instrumentation or sample preparation strategies (79, 122, 125–128). For example, expansion microscopy, a type of sample preparation that expands a sample along all axes so that the sample can be imaged in finer detail, has been used to prepare samples for hyperspectral SRS. This combination provided nanoscale spatial resolution of endogenous lipids (and other molecules) within a sample (126). SRS has been combined with fluorescence microscopy to yield a high-speed multiplexed imaging system with a temporal resolution of seconds that can track the dynamics of LDs in living cells (79). Notably, this system offered 20-color vibrational contrast with the ability to be increased to 26 colors, creating a powerful tool to investigate intracellular molecules. Because this compound instrument is also applicable to molecules other than lipids, single-cell multiomics becomes possible on a single platform. The use of Raman-active probes including photoactivatable probes further expands the utility of SRS imaging (82, 83, 106, 129, 130). Multicolor photoactivatable alkyne Raman reporters using cyclopropenone caging have been applied to image and track live cells (130). These light-activatable probes are relatively small compared with fluorescent probes and minimally perturb cellular physiology. The probes can be multiplexed with other methods providing multicomponent imaging while measuring cellular dynamics, for example, simultaneous imaging of mitochondria, lysosomes, and LDs.

3.3. Coherent Anti-Stokes Raman Scattering Imaging

As with SRS, CARS is a nonlinear optical process with submicron spatial resolution when applied to imaging single cells. The signal of CARS is up to 5 orders of magnitude stronger than that of spontaneous Raman scattering, and it is highly effective for detection of lipids (131). Compared with SRS, CARS has a simpler signal detection system since the emitted signal is at a different energy than that of the pump/probe scattered photons and so signal detection requires only spectral filters (64, 69, 91, 119). But CARS typically has a poorer signal-to-noise ratio compared with SRS, and the CARS signal is not proportional to analyte concentration (unlike the SRS signal), making CARS more challenging in terms of analyte quantification (84, 91, 119). CARS possesses an acquisition time 2 orders of magnitude lower than SRS (90). Although CARS and SRS both permit nondestructive imaging in a label-free manner, both methods can induce significant photodamage due to the high peak powers of the picosecond or femtosecond lasers. Like SRS, spatial resolutions in the hundreds of nanometers are achievable with CARS (65). These attributes have enabled CARS to have a tremendous impact on the field of single-cell lipid measurements, particularly in the dynamics of LDs (132–134). For example, recent technological innovations have enabled high-speed, submicron visualization of LD movements within single cells (132).

Enhancements in CARS instrumentation have yielded additional advances in multiplexed and hyperspectral imaging at high spatial resolution to enhance analyte identification in single cells, as well as the integration of CARS with other microscopy methods for multimodal imaging (86–89, 131, 135–141). As an example, hyperspectral CARS has been applied to assay lipids, proteins, and DNA in single osteosarcoma cells and to track their concentration changes over time during mitosis. A similar methodology was used to quantify lipid concentration and composition in individual LDs in living cells over time when supplied with a medium possessing different FAs (142). Multiplexed CARS permitting imaging over a range of wavelengths (or vibrational energies) and combined with fluorescence microscopy has enabled tracking of lipid storage in LDs versus the endoplasmic reticulum before and after receptor (TrkB) stimulation in living single colorectal cells (135). Other CARS advances include the use of more than two lasers to access a broader range of Raman bands, for example, broadband CARS (143), probing a wavelength range of >3000 cm^{-1} with a resolution of <10 cm^{-1} for assay of lipids in single murine pancreatic duct cells. Another compound microscope example is the integration of sum-frequency generation (SFG) imaging with CARS (136). In this instance, SFG imaging of an exogenously added dye enabled selective visualization of the plasma membrane of cells coupled to CARS-based visualization of cellular lipids in single neurons.

4. FLUORESCENCE-BASED TECHNOLOGIES

Fluorescence involves the absorption of a photon with excitation of a molecule from a ground electronic state into a higher energy electronic state (first or second excited singlet state). Energy then is dissipated by internal conversion with return to the lowest excited singlet state. Return to the ground state can occur by emission of a photon (fluorescence) now at a lower energy than that originally absorbed (144). Fluorescence-based measurements offer many advantages including high sensitivity and proportionality of fluorescence intensity to fluorophore concentration. The unique spectral properties of a fluorophore confer specificity in fluorophore identification as well as enabling multiplexed assays using multiple fluorophores. Additionally, a large number of fluorophores with a wide range of emission and excitation spectra are available. Fluorescence-based detection is compatible with a wide range of assay types often using simple, robust instrumentation. Fluorophores are readily conjugated to other molecules using a variety of chemistries. Major limitations of fluorescence-based measurements include fluorophore photodegradation or loss over time, environment (pH, solvent, etc.) sensitivity of the photon emission energy, and potential for quenching (return to ground state without fluorophore emission). Since cellular lipids are not typically fluorescent, a strategy to incorporate a fluorophore into the assay, that is, a labeling strategy, is also required. This section focuses on microscopy methods and microseparation techniques that use fluorescence as a component of the lipid detection strategy, with a focus on the quantification of the lipid species and lipid metabolic pathways in single cells.

4.1. Fluorescence Microscopy

Fluorescence microscopy of lipids offers significant advantages over other methods including the ease of accessibility and a wide range of available microscopy methods, for example, confocal, two-photon, light-sheet, and super-resolution microscopes. Fluorescence microscopy typically achieves high sensitivity to measure very low concentrations (nanomolar) of cellular lipids with a high signal-to-noise ratio and excellent spatial resolution (often submicron). Fluorescence labeling can be accomplished by using prelabeled lipids added to the cells, staining by immunofluorescence methods, employing lipid-binding or reactive fluorophores, or applying other strategies. These labeling methods, while highlighting the desired lipids, may also increase background noise

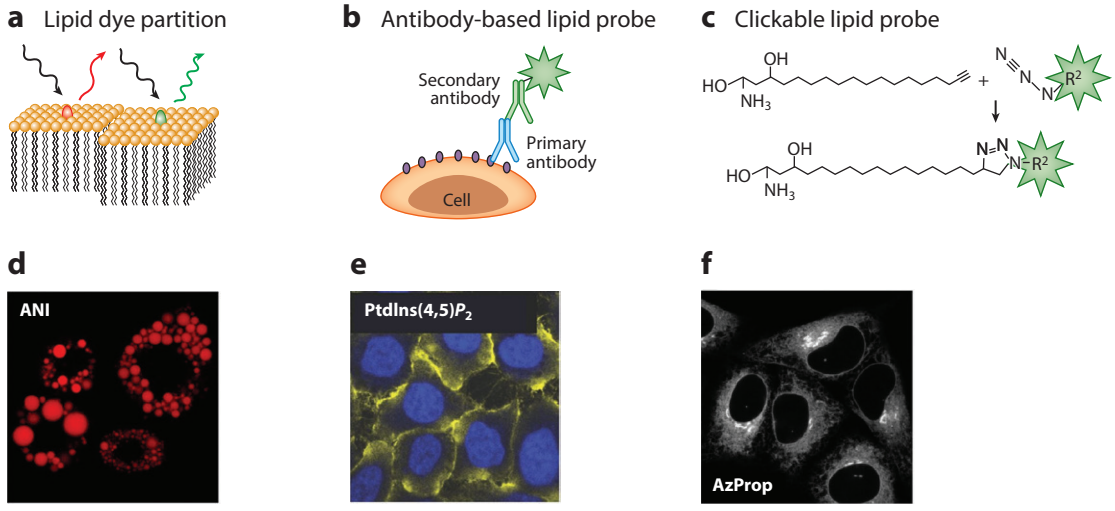

Figure 3

Fluorescence microscopy–based measurement of lipids. Schematics show the principles of (*a*) dyes that partition into lipids, (*b*) antibody-based lipid probes, and (*c*) clickable lipid probes. In panel *a*, the red and green ovals represent fluorophores of different wavelengths present in different membrane regions. In panels *b* and *c*, the green star depicts a fluorescent molecule placed onto an antibody or added via a click reaction. (*d*) Confocal laser scanning image of lipid droplets in preadipocyte cells stained by a solvatochromic probe. (*e*) Immunofluorescent staining of PtdIns(4,5)P_2 in HeLa cells. (*f*) The location of phospholipase D activity was highlighted by adding a clickable substrate to cells. The product formed was made visible using a clickable fluorophore. Panel *c* adapted with permission from Reference 4; copyright 2022 American Chemical Society. Panel *d* adapted with permission from Reference 154; copyright 2022 American Chemical Society. Panel *e* adapted with permission from Reference 172. Panel *f* adapted with permission from Reference 182; copyright 2017 American Chemical Society.

through nonspecific staining. Additionally, the reagents are critically dependent on their design for specificity as to the molecules labeled (with either high or low specificity possible). The methods frequently require the addition of exogenous reagents to cells, so the probes must be membrane permeant or the cells fixed to allow probe access to intracellular lipids. Another strategy is genetic engineering of cells to express protein constructs tagged with a fluorescent protein. In this section, we present three different fluorescence strategies to assay lipids in single cells: lipid partitioning reagents, lipid binding proteins, and functionalized lipids (**Figure 3**).

Cells possess a number of organelles such as LDs, lipid bodies, and other structures greatly enriched in lipid content relative to the majority of the intracellular environment. This attribute has been capitalized on through the use of hydrophobic dyes such as BODIPY 493/503, FD13, and Nile Red that, when added to cells, will partition into and mark these hydrophobic or other unique microenvironments (145–158) (**Figure 3*a***). Due to the very high concentration of dye loaded into the compartments, the signal sensitivity is exceptional, and spatial resolution of hundreds of nanometers is attainable for detailed imaging and tracking of these subcellular structures in living cells (152, 159). The use of molecules with differing partitioning behaviors and fluorescence properties also enables multiple structures to be tracked over time with minimal photodamage. Properly designed probes can report multiple attributes of the microenvironment including membrane fluidity, local polarity, lipid composition, domain sizes, and temporal properties (145–158, 160). Newer probes such as PIE-1 possess high fluorescence quantum yield and photostability, further improving upon measurement attributes for live cell imaging including imaging speed (147). Organelle-specific probes permit imaging of the polarity and lipid order in LDs, lysosomes, Golgi bodies, and mitochondria in the same cell (149). LD-specific probes with enhanced attributes have

also been developed for standard or two-photon imaging with high spatial resolution but low cellular toxicity (152, 158). Energy transfer between pairs of these dyes and/or other molecules can be used to investigate the degree of order or disorder in lipid domains and lipid packing in living cells (161, 162). For example, these types of studies have revealed that living cell membranes comprise a mixture of both ordered and disordered lipid domains (163). While these probes have enabled breakthrough advances in the understanding of lipid-rich subcellular organelles and their structure, the lack of specificity of the probes in terms of labeling specific lipid species has limited their application.

Protein-based staining reagents such as antibodies and binding domains have long been a mainstay for protein identification or sensors in single cells and have been used with success for lipids (164–172) (**Figure 3*b***). Antibodies have the advantage of being easy-to-apply reagents using standard protocols and are often commercially available. However, raising antibodies against lipids can be quite challenging due to their hydrophobic character and ubiquitous presence throughout species (lessening their immunogenicity). Antibodies can be very specific for the targeted molecule, but a well-recognized challenge with antibodies is that they often bind to molecules other than the intended target. Immunofluorescence-based probes have been used most often to assay phosphoinositide and sphingolipid location within single cells (171). An advantage of these reagents is the ability to perform multiplexed assays by also simultaneously performing immunofluorescence labeling of proteins, organelle markers, and other fluorescent probes with complementary spectral properties. Genetic engineering of cells to express lipid binding domains (subunits of a larger protein) linked to a fluorescence protein (enhanced green fluorescent protein or others) also have found success. For example, a peptide-based sensor was developed to detect anionic phospholipids in live HeLa cells, an approach that was compatible with two-photon excitation (167).

One strategy to improve the specificity of lipid probes is to label or functionalize the lipids themselves and then incorporate these labeled molecules into the cells to assay lipid localization, metabolism, transport, compartmentalization, and other properties within single cells (**Figure 3*c***). A wide array of fluorescently labeled or otherwise functionalized (biotinylated, photoactivatable, clickable, etc.) lipids are now commercially available (173–175). These probes have the advantage of having a known molecular structure and often undergoing some but not all endogenous metabolic reactions of the native molecule. A challenge, however, can be the efficient loading of these molecules into cells given the poor water solubility of lipids, although carriers such as polyamines and dispersants have been used to facilitate lipid delivery to cells (173–175). Exogenous loading can lead to mislocalization of these lipids; nevertheless, the use of these functionalized lipids has led to many novel insights into cellular lipid biology. An example is the use of BODIPY FL Ganglioside GM1 to label, characterize, and track lipid rafts in the plasma membrane of cells (176). Fluorescent sphingomyelin analogs also were developed to investigate the formation and function of raft domains (175). A mitochondrial-specific photoactivatable sphingosine has been used to show the rapid conversion of sphingosine into sphingosine-1 phosphate in HeLa cells (174). An obstacle present for all fluorescent lipids is the presence of the bulky fluorophore that can block binding to intracellular proteins including metabolic enzymes. A significant innovation addressing these impediments is the development of click lipids (177–182). Instead of a bulky fluorescent moiety, these reagents possess either a small azido group or a terminal alkyne, making the click lipids structurally very close to the endogenous counterpart (180, 183). The fluorophore used for detection is then added at experimental completion, enabling the click lipid to participate in normal cellular physiology. For example, an alkyne-oleate probe was used to track FA metabolism in cells and then clicked with an azide fluorophore (184). Azidoalcohols can be used in the phospholipase D–catalyzed transphosphatidylation reaction to produce azidolipids that can

then be fluorescently labeled to track the subcellular location of phospholipase D activity and PA production (182). A related activity-based imaging strategy employs cyclooctene-containing primary alcohols to act as a nucleophile in the phospholipase D reaction, with phosphatidylcholine providing near real-time imaging of PA production in living cells (181, 182).

CE: capillary electrophoresis

4.2. Fluorescence-Based Microseparation Methods

Many separation techniques have been applied to assay single cells, including TLC, capillary electrophoresis (CE), and even HPLC (4, 185–188). To date, CE is the most prevalent method used for lipid assays in single cells, with TLC as an emerging technique. With CE, analytes are separated in a solvent (typically aqueous) under an electric field. The dominant parameter for separation is the charge-to-mass ratio of the analytes, although other separation strategies are possible, such as micellar electrokinetic chromatography, which separates analytes on the basis of partitioning into micelles while under an electric field (185). In contrast, TLC separation relies on the capillary forces of an organic solvent moving through a matrix (typically silica based) and separates analytes on the basis of their differential interactions with the matrix and organic solvent (189). Separation techniques have common advantages in lipid analysis. The methods typically have low background noise because the analyte is separated from other cellular material at the time of detection. The separation step also provides some degree of specificity because different analytes will possess characteristic migration times or arrival times at the detection zone. CE provides exceptionally high resolution (peak capacities of 50–100 peaks/separation), separation efficiency (>1 million theoretical plates), and sensitivity ($\leq 10^{-21}$ mol or $\leq$1 nM in a 1-pL cell) (185). Some CE systems have even achieved limits of detection of 10^{-23} mol (190). Use of multiple fluorophores with different spectral properties further increases the number of analytes that can be simultaneously measured in CE. As long as the analytes remain fluorescent, CE can be used to track downstream metabolites as they form from a reporter molecule (4, 187). Single-cell lipid assays by CE can also be fully automated and integrated with microscopy methods (185). Microfluidic-based CE assays enable further integration and miniaturization of complete workflows. TLC, on the other hand, offers the major advantages of low cost and ease of accessibility but possesses low resolution and separation (189). However, both CE and TLC applied to single-cell lipid assays have drawbacks. Measuring endogenous lipids in cell samples using CE and fluorescence is quite difficult, because lipids are not typically fluorescent and would need to be derivatized prior to detection. For this reason, both methods use a prelabeled substrate that is loaded into the cells, and this loading step can be facile or quite challenging depending on the properties of the molecule. Both techniques are cell destructive and consume the cellular contents, prohibiting multiplexing of CE- or TLC-based single-cell lipid assays with additional downstream assays. Additionally, this limitation means that, for the most part, the methods do not possess a subcellular spatial resolution. Finally, most of the demonstrated technologies for single-cell lipid assays are moderate in throughput ($\leq$5 cells/min), at best (4, 185).

For CE, the ability to measure multiple lipid metabolites from a single cell has enabled fundamental investigations into cell-to-cell heterogeneity in signaling behavior as well as responses to drugs (4, 185, 186) (**Figure 4*a***). Sphingolipids, glycosphingolipids, and phosphoinositides as well as ganglioside metabolic pathways have been assessed in single cells by CE (185, 186, 191, 192). For example, when cells were loaded with sphingosine fluorescein and then assayed by CE, more than five metabolic products could be identified in cells, with sphingosine-1-phosphate fluorescein and hexadecimal fluorescein composing the majority of products formed. Most interesting is that the single cells readily clustered into two groups: one group of cells with high SK activity and one group with low SK activity (186). After loading with a fluorescent lipid, single cells can

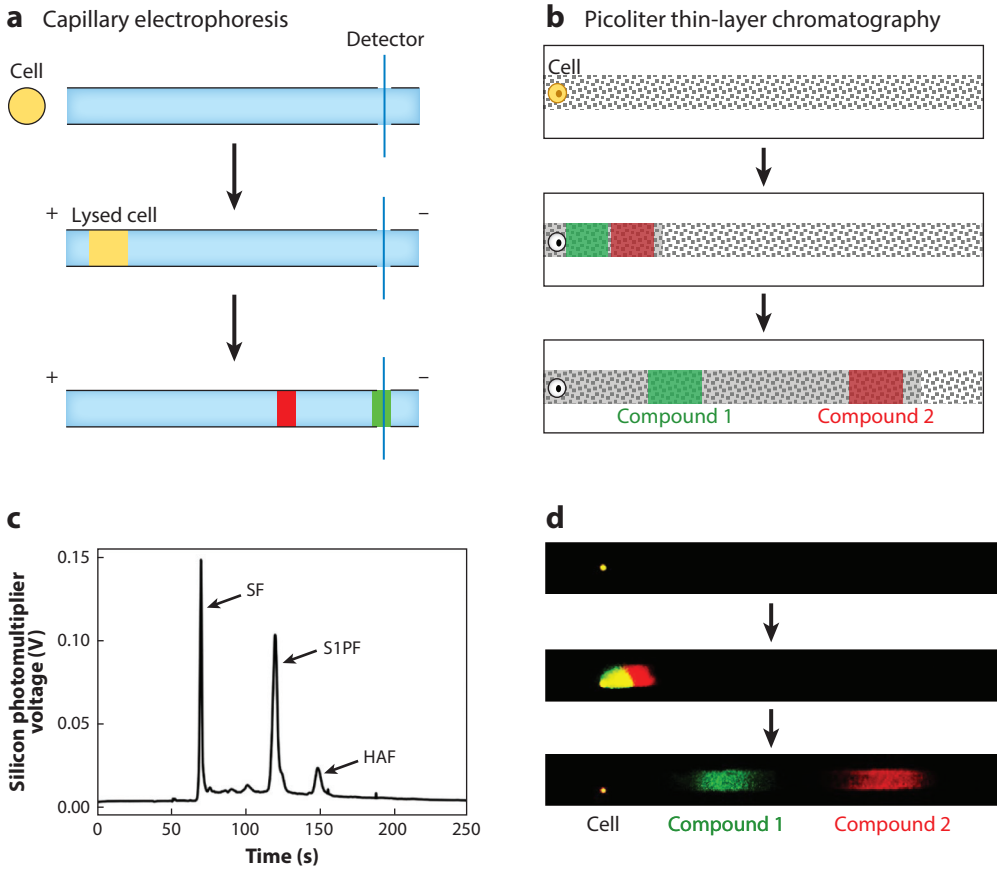

Figure 4

Fluorescence-based separation techniques for single-cell lipid assays. The schematics show the separation of cellular analytes using (*a*) capillary electrophoresis (CE) and (*b*) picoliter thin-layer chromatography (pTLC). (*c*) An electropherogram of the CE separation from a single leukemia cell loaded with sphingosine fluorescein (SF) is shown. Sphingosine kinase activity was measured by quantifying the conversion of reporter SF to downstream metabolites, sphingosine-1-phosphate fluorescein (S1PF) or hexadecenoic acid fluorescein (HAF). (*d*) A single leukemic cell was loaded with 3,3′-dioctadecyloxacarbocyanine perchlorate (DiO) and 1,1′-dioctadecyl-3,3,3′,3′-tetramethylindodicarbocyanine, 4-chlorobenzenesulfonate salt (DiD), and the cell was assayed by pTLC. Panels *b* and *d* adapted with permission from Reference 195; copyright 2022 American Chemical Society. Panel *c* adapted with permission from Reference 185; copyright 2020 American Chemical Society.

be assayed while living, as in the prior example, or fixed and stored prior to assaying because the lipids remain partitioned in the fixed cells (187, 192, 193). The bulky fluorophore placed on the lipids can alter lipid location and metabolism in cells, and recent studies have used click lipids for assay of single-cell lipid metabolism. In this strategy, termed fix and click, cells are loaded with a clickable lipid, and after incubation for varying times with or without agonists or inhibitors, the cells are fixed, and the click reaction is performed to create fluorescent analytes from the intracellular molecules possessing the clickable moiety (4). This strategy enables the tracking of signal pathway activity in single cells by CE using a near-native lipid substrate loaded into cells with greater measurement fidelity.

To overcome the throughput and cost limitations of CE, several groups have worked to improve the rates of both serial and parallel throughput to increase the number of cells that can be assayed,

as well as to automate and diminish instrument costs. For example, a system with a hybrid CE-microfluidic device (**Figure 4*b***) enabled 100 cells placed on an array to be sequentially and rapidly assayed with a sensitivity of 10^{-21} mol and a throughput of 3.5 cells/min (186, 191). A parallel CE system with an array of five capillaries coupled to an array of microwells demonstrated the simultaneous separation of ceramides and gangliosides from single cells (194). This system was also adapted to incorporate a multicolored fluorescence detection system to further expand the numbers of detectable analytes and simultaneously assay glycolipid catabolism and anabolism from a single cell with detection limits of 10^{-22} to 10^{-23} mol (188, 192). Other innovations developed low-cost ($130) yet highly sensitive detection systems using silicon photomultipliers (185).

In the past TLC has been viewed as a low-sensitivity method requiring large sample volumes (10^{-7} L) and thus not suitable for assay of a 1-pL volume cell. This is due in part to the plate-based format (centimeters in length and width, with a depth of ~100–250 μm) for TLC, which enables diffusional spreading (or dilution) of analytes in three dimensions. Recent innovations in the microfabrication of arrays of miniature TLC separation lanes or picoliter thin-layer chromatography (pTLC) have created opportunities for assay of lipids in single cells (195). Microchannels (width ~50 μm and depth ~13 μm) were fabricated on a surface and then filled with a monolithic microporous silica gel to confine the movement of analytes along the microchannels, limiting diffusion to one dimension. These devices enable the TLC-based separation of picoliter to nanoliter volume samples with excellent fluorescence detection limits. When single cells loaded with fluorescent lipids, for example, a fluorescent sphingosine, were spotted at the entryway of the microchannels and TLC was initiated, the lipid and its downstream metabolites (ceramide and sphingosine-1-phosphate) were detectable. While the separation resolution is low (~2–4) compared with CE, the advantages of the pTLC platform are its operational simplicity, the minimal equipment needs, and its robustness, making the technology suitable for many applications, including single-cell assays of lipases and lipid kinases.

5. CONCLUSION

Single-cell omics is progressing rapidly, with impressive technological developments in the past decade in proteomics, genomics, and transcriptomics. These high-throughput technologies have revealed fundamentally new insights into cell physiology. Given the importance of lipids in both health and disease, understanding the full range of lipids within a single cell is increasingly critical, as has now become possible with other cellular constituents. These attributes include not only lipid chemical identity and spatial and temporal distribution but also the flow of signals through the various lipid pathways. This review covers the impressive advances that have been made in the measurement of lipids from a single cell, including innovations in mass spectrometry, Raman microscopy, fluorescence microscopy, and microseparation methods (**Table 1**). These methods are in general complementary in their properties, with some providing high spatial or temporal resolution, excellent specificity, precise quantification, impressive sensitivity, or multiplexed lipid measurements, yet none of the methods possess all of the desired characteristics. This is largely due to the challenges in lipid measurement (hydrophobicity and chemical diversity) combined with the extremely small size of a typical mammalian cell and the wide concentration range of lipid species within a cell.

While the techniques in this review have revolutionized our understanding of the lipid composition and physiology within single cells, additional analytical needs in single-cell lipid assays remain. Since many cellular samples are ultralow volume (from femtoliter vesicles to picoliter cells) and many signaling lipids can be present at less than 10^{-20} mol per cell, sensitivity remains a challenge for most methods. Strategies to increase sample throughput while maintaining the ease of sample introduction and analyte sensitivity are an opportunity ripe for innovation, especially

Table 1 Summary of approximate lipid metrics achieved for the different analytical techniques

Feature/technique	Spatial resolution	Sensitivity	Sample destruction	Ease of access	Specificity (molecular identification)
MALDI-MS	1–5 μm	10^{-15}–10^{-18} moles	Yes	Low-medium	Excellent
ESI-MS	10–100 μm	10^{-15}–10^{-17} moles	Yes	Low-medium	Excellent
SI-MS	0.05–1.0 μm	10^{-15}–10^{-17} moles	Yes	Low-medium	Excellent
Spontaneous Raman imaging	0.3–0.6 μm	1–10 mM	No	Medium	Poor
SRS	0.1–2 μm	0.1–10 mM	No	Medium	Poor
CARS	0.1 μm	0.1–10 mM	No	Medium	Poor
Fluorescence microscopy	0.2–1 μm	$\leq 10^{-18}$ moles	No	High	Intermediate
Microseparation methods	Whole cell (~10 μm)	10^{-21} moles	Yes	Low-medium	Intermediate

Abbreviations: CARS, coherent anti-Stokes Raman scattering; ESI-MS, electrospray ionization mass spectrometry; MALDI-MS, matrix-assisted laser desorption/ionization mass spectrometry; SI-MS, secondary-ion mass spectrometry; SRS, stimulated Raman scattering.

in pharmaceutical applications. A major barrier yet to be overcome by most of the technologies is ease of use, since most techniques require expertise in the instrumentation and sample preparation methods. For example, the majority of instruments described are best suited to placement in core facilities due to either cost or required expertise, creating opportunities in the future for the introduction of simple cassettes and kits for the nonexpert to further democratize single-cell lipid assays. There remain enormous opportunities for engineers, biologists, and chemists to develop improved technologies, propelling the field of single-cell lipidomics to new heights and rivaling the assays performed in the other omics fields.

DISCLOSURE STATEMENT

N.L.A. is an inventor of pTLC (PCT/US2022/019103). N.L.A. and M.Y. disclose a financial interest in Piccolo Biosystems, Inc. M.V. discloses no conflicts of interest.

ACKNOWLEDGMENTS

This work was supported by the National Institutes of Health under Award CA233811 and CA224763. The authors thank Gregery Woss for his assistance with illustrations.

LITERATURE CITED

1. Cockcroft S. 2021. Mammalian lipids: structure, synthesis and function. *Essays Biochem.* 65:813–45
2. Fahy E, Subramaniam S, Brown HA, Glass CK, Merrill AH, et al. 2018. A comprehensive classification system for lipids. In *Handbook of Biochemistry and Molecular Biology*, ed. RL Lundblad, FM Macdonald, pp. 298–321. Boca Raton, FL: CRC Press. 5th ed.
3. Olzmann JA, Carvalho P. 2019. Dynamics and functions of lipid droplets. *Nat. Rev. Mol. Cell Biol.* 20(3):137–55
4. Gallion LA, Wang Y, Massaro A, Yao M, Petersen BV, Zhang Q, et al. 2022. "Fix and click" for assay of sphingolipid signaling in single primary human intestinal epithelial cells. *Anal. Chem.* 94(3):1594–600
5. Hussain G, Anwar H, Rasul A, Imran A, Qasim M, et al. 2020. Lipids as biomarkers of brain disorders. *Crit. Rev. Food Sci. Nutr.* 60(3):351–74

6. Dumas F, Haanappel E. 2017. Lipids in infectious diseases—the case of AIDS and tuberculosis. *Biochim. Biophys. Acta Biomembr.* 1859(9):1636–47
7. Liu Q, Luo Q, Halim A, Song G. 2017. Targeting lipid metabolism of cancer cells: a promising therapeutic strategy for cancer. *Cancer Lett.* 401:39–45
8. Kohno S, Keenan AL, Ntambi JM, Miyazaki M. 2018. Lipidomic insight into cardiovascular diseases. *Biochem. Biophys. Res. Commun.* 504(3):590–95
9. Perrotti F, Rosa C, Cicalini I, Sacchetta P, Del Boccio P, et al. 2016. Advances in lipidomics for cancer biomarkers discovery. *Int. J. Mol. Sci.* 17(12):1992
10. Snaebjornsson MT, Janaki-Raman S, Schulze A. 2020. Greasing the wheels of the cancer machine: the role of lipid metabolism in cancer. *Cell Metab.* 31(1):62–76
11. Fhu CW, Ali A. 2020. Fatty acid synthase: an emerging target in cancer. *Molecules* 25(17):3935
12. Sun W, Li P, Cai J, Ma J, Zhang X, et al. 2022. Lipid metabolism: immune regulation and therapeutic prospectives in systemic lupus erythematosus. *Front. Immunol.* 13:860586
13. Bernardi S, Marcuzzi A, Piscianz E, Tommasini A, Fabris B. 2018. The complex interplay between lipids, immune system and interleukins in cardio-metabolic diseases. *IJMS* 19(12):4058
14. Liu Q, Ge W, Wang T, Lan J, Martínez-Jarquín S, et al. 2021. High-throughput single-cell mass spectrometry reveals abnormal lipid metabolism in pancreatic ductal adenocarcinoma. *Angew. Chem.* 133(46):24739–47
15. Rajbhandari P, Arneson D, Hart SK, Ahn IS, Diamante G, et al. 2019. Single cell analysis reveals immune cell-adipocyte crosstalk regulating the transcription of thermogenic adipocytes. *eLife* 8:e49501
16. Sethi S, Brietzke E. 2017. Recent advances in lipidomics: analytical and clinical perspectives. *Prostaglandins Other Lipid Mediat.* 128:8–16
17. Feider CL, Krieger A, DeHoog RJ, Eberlin LS. 2019. Ambient ionization mass spectrometry: recent developments and applications. *Anal. Chem.* 91(7):4266–90
18. Liu R, Pan N, Zhu Y, Yang Z. 2018. T-probe: an integrated microscale device for online in situ single cell analysis and metabolic profiling using mass spectrometry. *Anal. Chem.* 90(18):11078–85
19. Duncan KD, Fyrestam J, Lanekoff I. 2019. Advances in mass spectrometry based single-cell metabolomics. *Analyst* 144(3):782–93
20. Huang L, Fang M, Cupp-Sutton KA, Wang Z, Smith K, Wu S. 2021. Spray-capillary-based capillary electrophoresis mass spectrometry for metabolite analysis in single cells. *Anal. Chem.* 93(10):4479–87
21. Van Acker T, Buckle T, Van Malderen SJ, van Willigen DM, van Unen V, et al. 2019. High-resolution imaging and single-cell analysis via laser ablation-inductively coupled plasma-mass spectrometry for the determination of membranous receptor expression levels in breast cancer cell lines using receptor-specific hybrid tracers. *Anal. Chim. Acta* 1074:43–53
22. Vaysse PM, Heeren RM, Porta T, Balluff B. 2017. Mass spectrometry imaging for clinical research—latest developments, applications, and current limitations. *Analyst* 142(15):2690–712
23. Capolupo L, Khven I, Lederer AR, Mazzeo L, Glousker G, et al. 2022. Sphingolipid control dermal fibroblast heterogeneity. *Science* 376(6590):eabh1623
24. Yin L, Zhang Z, Liu Y, Gao Y, Gu J. 2019. Recent advances in single-cell analysis by mass spectrometry. *Analyst* 144(3):824–45
25. Dueñas ME, Essner JJ, Lee YJ. 2017. 3D MALDI mass spectrometry imaging of a single cell: spatial mapping of lipids in the embryonic development of zebrafish. *Sci. Rep.* 7(1):14946
26. Leopold J, Popkova Y, Engel KM, Schiller J. 2018. Recent developments of useful MALDI matrices for the mass spectrometric characterization of lipids. *Biomolecules* 8(4):173
27. Marsico TV, de Sousa Sales JN, Ferreira CR, Sudano MJ, Viana JHM, et al. 2021. Characteristic MALDI-MS lipid profiles of Gir, Holstein and crossbred (Gir x Holstein) oocytes recovered by ovum pick-up. *Livestock Sci.* 243:104380
28. Agüi-Gonzalez P, Jähne S, Phan NT. 2019. SIMS imaging in neurobiology and cell biology. *J. Anal. At. Spectrom.* 34(7):1355–68
29. Schnackenberg LK, Thorn DA, Barnette D, Jones EE. 2022. MALDI imaging mass spectrometry: an emerging tool in neurology. *Metab. Brain Dis.* 37(1):105–21
30. Niehaus M, Soltwisch J, Belov ME, Dreisewerd K. 2019. Transmission-mode MALDI-2 mass spectrometry imaging of cells and tissues at subcellular resolution. *Nat. Methods* 16(9):925–31

31. Martín-Saiz L, Mosteiro L, Solano-Iturri JD, Rueda Y, Martín-Allende J, et al. 2021. High-resolution human kidney molecular histology by imaging mass spectrometry of lipids. *Anal. Chem.* 93:9364–72
32. Xie W, Gao D, Jin F, Jiang Y, Liu H. 2015. Study of phospholipids in single cells using an integrated microfluidic device combined with matrix-assisted laser desorption/ionization mass spectrometry. *Anal. Chem.* 87(14):7052–59
33. Yang T, Gao D, Jin F, Jiang Y, Liu H. 2016. Surface-printed microdot array chips coupled with matrix-assisted laser desorption/ionization mass spectrometry for high-throughput single-cell patterning and phospholipid analysis: surface-printed microdot array chips coupled with MALDI-TOF MS. *Rapid. Commun. Mass. Spectrom.* 30:73–79
34. Neumann EK, Ellis JF, Triplett AE, Rubakhin SS, Sweedler JV. 2019. Lipid analysis of 30 000 individual rodent cerebellar cells using high-resolution mass spectrometry. *Anal. Chem.* 91(12):7871–78
35. Neumann EK, Comi TJ, Rubakhin SS, Sweedler JV. 2019. Lipid heterogeneity between astrocytes and neurons revealed by single-cell MALDI-MS combined with immunocytochemical classification. *Angew. Chem.* 131(18):5971–75
36. Yang B, Patterson NH, Tsui T, Caprioli RM, Norris JL. 2018. Single-cell mass spectrometry reveals changes in lipid and metabolite expression in RAW 264.7 cells upon lipopolysaccharide stimulation. *J. Am. Soc. Mass Spectrom.* 29(5):1012–20
37. Do TD, Ellis JF, Neumann EK, Comi TJ, Tillmaand EG, et al. 2018. Optically guided single cell mass spectrometry of rat dorsal root ganglia to profile lipids, peptides and proteins. *ChemPhysChem* 19(10):1180–91
38. Zenobi R. 2013. Single-cell metabolomics: analytical and biological perspectives. *Science* 342(6163):1243259
39. Pan N, Rao W, Kothapalli NR, Liu R, Burgett AW, Yang Z. 2014. The single-probe: a miniaturized multifunctional device for single cell mass spectrometry analysis. *Anal. Chem.* 86(19):9376–80
40. Li Z, Cheng S, Lin Q, Cao W, Yang J, et al. 2021. Single-cell lipidomics with high structural specificity by mass spectrometry. *Nat. Commun.* 12(1):2869
41. Chen F, Lin L, Zhang J, He Z, Uchiyama K, Lin JM. 2016. Single-cell analysis using drop-on-demand inkjet printing and probe electrospray ionization mass spectrometry. *Anal. Chem.* 88(8):4354–60
42. Zhu Y, Wang W, Yang Z. 2020. Combining mass spectrometry with Paternò-Büchi reaction to determine double-bond positions in lipids at the single-cell level. *Anal. Chem.* 92(16):11380–87
43. Cahill JF, Riba J, Kertesz V. 2019. Rapid, untargeted chemical profiling of single cells in their native environment. *Anal. Chem.* 91(9):6118–26
44. Pedro L, Rudewicz PJ. 2020. Analysis of live single cells by confocal microscopy and high-resolution mass spectrometry to study drug uptake, metabolism, and drug-induced phospholipidosis. *Anal. Chem.* 92(24):16005–15
45. Hiyama E, Ali A, Amer S, Harada T, Shimamoto K, et al. 2015. Direct lipido-metabolomics of single floating cells for analysis of circulating tumor cells by live single-cell mass spectrometry. *Anal. Sci.* 31(12):1215–17
46. Xu ST, Yang C, Yan XP. 2021. Nanothorn filter-facilitated online cell lysis for rapid and deep intracellular profiling by single-cell mass spectrometry. *Anal. Chem.* 93(47):15677–86
47. Merrill CB, Basit A, Armirotti A, Jia Y, Gall CM, et al. 2017. Patch clamp-assisted single neuron lipidomics. *Sci. Rep.* 7(1):5318
48. Wang R, Zhao H, Zhang X, Zhao X, Song Z, Ouyang J. 2019. Metabolic discrimination of breast cancer subtypes at the single-cell level by multiple microextraction coupled with mass spectrometry. *Anal. Chem.* 91(5):3667–74
49. Zhao Y, Chen Z, Wu Y, Tsukui T, Ma X, et al. 2019. Separating and profiling phosphatidylcholines and triglycerides from single cellular lipid droplet by in-tip solvent microextraction mass spectrometry. *Anal. Chem.* 91(7):4466–71
50. Sun M, Yang Z. 2018. Metabolomic studies of live single cancer stem cells using mass spectrometry. *Anal. Chem.* 91(3):2384–91
51. Bergman HM, Lanekoff I. 2017. Profiling and quantifying endogenous molecules in single cells using nano-DESI MS. *Analyst* 142(19):3639–47

52. Xi Y, Tu A, Muddiman DC. 2020. Lipidomic profiling of single mammalian cells by infrared matrix-assisted laser desorption electrospray ionization (IR-MALDESI). *Anal. Bioanal. Chem.* 412(29):8211–22
53. Zhang L, Xu T, Zhang J, Wong SCC, Ritchie M, et al. 2021. Single cell metabolite detection using inertial microfluidics-assisted ion mobility mass spectrometry. *Anal. Chem.* 93(30):10462–68
54. Yao H, Zhao H, Zhao X, Pan X, Feng J, et al. 2019. Label-free mass cytometry for unveiling cellular metabolic heterogeneity. *Anal. Chem.* 91(15):9777–83
55. Liu A, Zhang H, Ding J, Kou W, Yan F, et al. 2020. Enrichment of phospholipids using magnetic Fe_3O_4/TiO_2 nanoparticles for quantitative detection at single cell levels by electrospray ionization mass spectrometry. *Talanta* 212:120769
56. Popczun NJ, Breuer L, Wucher A, Winograd N. 2017. On the SIMS ionization probability of organic molecules. *J. Am. Soc. Mass Spectrom.* 28(6):1182–91
57. Sheng L, Cai L, Wang J, Li Z, Mo Y, et al. 2017. Simultaneous imaging of newly synthesized proteins and lipids in single cell by TOF-SIMS. *Int. J. Mass Spectrom.* 421:238–44
58. Hua X, Li HW, Long YT. 2018. Investigation of silver nanoparticle induced lipids changes on a single cell surface by time-of-flight secondary ion mass spectrometry. *Anal. Chem.* 90(2):1072–76
59. Shao C-F, Zhao Y, Wu K, Jia F-F, Luo Q, et al. 2018. Correlated secondary ion mass spectrometry-laser scanning confocal microscopy imaging for single cell-principles and applications. *Chinese J. Anal. Chem.* 46(7):1005–16
60. Waki M, Ide Y, Ishizaki I, Nagata Y, Masaki N, et al. 2014. Single-cell time-of-flight secondary ion mass spectrometry reveals that human breast cancer stem cells have significantly lower content of palmitoleic acid compared to their counterpart non-stem cancer cells. *Biochimie* 107:73–77
61. Milijaš Jotić M, Panevska A, Iacovache I, Kostanjšek R, Mravinec M, et al. 2021. Dissecting out the molecular mechanism of insecticidal activity of ostreolysin A6/pleurotolysin B complexes on Western corn rootworm. *Toxins* 13:455
62. Do TD, Comi TJ, Dunham SJ, Rubakhin SS, Sweedler JV. 2017. Single cell profiling using ionic liquid matrix-enhanced secondary ion mass spectrometry for neuronal cell type differentiation. *Anal. Chem.* 89(5):3078–86
63. He C, Fong LG, Young SG, Jiang H. 2017. NanoSIMS imaging: an approach for visualizing and quantifying lipids in cells and tissues. *J. Investig. Med.* 65(3):669–72
64. Zhang C, Zhang D, Cheng JX. 2015. Coherent Raman scattering microscopy in biology and medicine. *Annu. Rev. Biomed. Eng.* 17:415–45
65. Tipping WJ, Lee M, Serrels A, Brunton VG, Hulme AN. 2016. Stimulated Raman scattering microscopy: an emerging tool for drug discovery. *Chem. Soc. Rev.* 45(8):2075–89
66. Gomes da Costa S, Richter A, Schmidt U, Breuninger S, Hollricher O. 2019. Confocal Raman microscopy in life sciences. *Morphologie* 103(341):11–16
67. Müller M, Zumbusch A. 2007. Coherent anti-Stokes Raman scattering microscopy. *ChemPhysChem* 8(15):2156–70
68. Eberhardt K, Stiebing C, Matthäus C, Schmitt M, Popp J. 2015. Advantages and limitations of Raman spectroscopy for molecular diagnostics: an update. *Expert Rev. Mol. Diagnost.* 15(6):773–87
69. Yue S, Cheng JX. 2016. Deciphering single cell metabolism by coherent Raman scattering microscopy. *Curr. Opin. Chem. Biol.* 33:46–57
70. Yu Y, Ramachandran PV, Wang MC. 2014. Shedding new light on lipid functions with CARS and SRS microscopy. *Biochim. Biophys. Acta Mol. Cell Biol. Lipids* 1841(8):1120–29
71. Li S, Li Y, Yi R, Liu L, Qu J. 2020. Coherent anti-Stokes Raman scattering microscopy and its applications. *Front. Phys.* 8:598420
72. Kang JW, Nguyen FT, Lue N. 2021. Temporal imaging of live cells by high-speed confocal Raman microscopy. *Materials* 14(13):3732
73. Xu Y, Hou X, Zhu Q, Mao S, Ren J, et al. 2022. Phenotype identification of HeLa cells knockout CDK6 gene based on label-free Raman imaging. *Anal. Chem.* 94(25):8890–98
74. Surmacki JM, Quiros-Gonzalez I, Bohndiek SE. 2022. Evaluation of label-free confocal Raman microspectroscopy for monitoring oxidative stress in vitro in live human cancer cells. *Antioxidants* 11(3):573

75. Roman M, Wrobel TP, Panek A, Paluszkiewicz C, Kwiatek WM. 2020. Lipid droplets in prostate cancer cells and effect of irradiation studied by Raman microspectroscopy. *Biochim. Biophys. Acta Mol. Cell Biol. Lipids* 1865(9):158753
76. Uematsu M, Shimizu T. 2021. Raman microscopy-based quantification of the physical properties of intracellular lipids. *Commun. Biol.* 4(1):1176
77. Beton K, Wysocki P, Brozek-Pluska B. 2022. Mevastatin in colon cancer by spectroscopic and microscopic methods—Raman imaging and AFM studies. *Spectrochim. Acta A Mol. Biomol. Spectrosc.* 270:120726
78. Feuerer N, Marzi J, Brauchle EM, Carvajal Berrio DA, Billing F, et al. 2021. Lipidome profiling with Raman microspectroscopy identifies macrophage response to surface topographies of implant materials. *PNAS* 118(52):e2113694118
79. Shou J, Oda R, Hu F, Karasawa K, Nuriya M, et al. 2021. Super-multiplex imaging of cellular dynamics and heterogeneity by integrated stimulated Raman and fluorescence microscopy. *iScience* 24(8):102832
80. Lita A, Kuzmin AN, Pliss A, Baev A, Rzhevskii A, et al. 2019. Toward single-organelle lipidomics in live cells. *Anal. Chem.* 91(17):11380–87
81. Wei L, Chen Z, Shi L, Long R, Anzalone AV, et al. 2017. Super-multiplex vibrational imaging. *Nature* 544(7651):465–70
82. Hu F, Zeng C, Long R, Miao Y, Wei L, et al. 2018. Supermultiplexed optical imaging and barcoding with engineered polyynes. *Nat. Methods* 15(3):194–200
83. Wei L, Hu F, Shen Y, Chen Z, Yu Y, et al. 2014. Live-cell imaging of alkyne-tagged small biomolecules by stimulated Raman scattering. *Nat. Methods* 11(4):410–12
84. Lima C, Muhamadali H, Goodacre R. 2021. The role of Raman spectroscopy within quantitative metabolomics. *Annu. Rev. Anal. Chem.* 14:323–45
85. Figueroa B, Fu W, Nguyen T, Shin K, Manifold B, et al. 2018. Broadband hyperspectral stimulated Raman scattering microscopy with a parabolic fiber amplifier source. *Biomed. Opt. Express* 9(12):6116–31
86. Boorman D, Pope I, Masia F, Langbein W, Hood S, et al. 2021. Hyperspectral CARS microscopy and quantitative unsupervised analysis of deuterated and non-deuterated fatty acid storage in human cells. *J. Chem. Phys.* 155(22):224202
87. Nahmad-Rohen A, Regan D, Masia F, McPhee C, Pope I, et al. 2020. Quantitative label-free imaging of lipid domains in single bilayers by hyperspectral coherent Raman scattering. *Anal. Chem.* 92(21):14657–66
88. Masia F, Pope I, Watson P, Langbein W, Borri P. 2018. Bessel-beam hyperspectral CARS microscopy with sparse sampling: enabling high-content high-throughput label-free quantitative chemical imaging. *Anal. Chem.* 90(6):3775–85
89. Karuna A, Masia F, Wiltshire M, Errington R, Borri P, Langbein W. 2019. Label-free volumetric quantitative imaging of the human somatic cell division by hyperspectral coherent anti-Stokes Raman scattering. *Anal. Chem.* 91(4):2813–21
90. Syed A, Smith EA. 2017. Raman imaging in cell membranes, lipid-rich organelles, and lipid bilayers. *Annu. Rev. Anal. Chem.* 10:271–91
91. Manifold B, Fu D. 2022. Quantitative stimulated Raman scattering microscopy: promises and pitfalls. *Annu. Rev. Anal. Chem.* 15:269–89
92. Szafraniec E, Kus E, Wislocka A, Kukla B, Sierka E, et al. 2019. Raman spectroscopy-based insight into lipid droplets presence and contents in liver sinusoidal endothelial cells and hepatocytes. *J. Biophoton.* 12(4):e201800290
93. Denbigh JL, Perez-Guaita D, Vernooij RR, Tobin MJ, Bambery KR, et al. 2017. Probing the action of a novel anti-leukaemic drug therapy at the single cell level using modern vibrational spectroscopy techniques. *Sci. Rep.* 7(1):2649
94. Kochan K, Maslak E, Krafft C, Kostogrys R, Chlopicki S, Baranska M. 2015. Raman spectroscopy analysis of lipid droplets content, distribution and saturation level in non-alcoholic fatty liver disease in mice. *J. Biophoton* 8(7):597–609
95. Tott S, Grosicki M, Glowacz J, Mohaissen T, Wojnar-Lason K, et al. 2021. Raman imaging-based phenotyping of murine primary endothelial cells to identify disease-associated biochemical alterations. *Biochim. Biophys. Acta Mol. Basis Dis.* 1867(9):166180

96. Janik-Olchawa N, Drozdz A, Wajda A, Sitarz M, Planeta K, et al. 2022. Biochemical changes of macrophages and U87MG cells occurring as a result of the exposure to iron oxide nanoparticles detected with the Raman microspectroscopy. *Spectrochim. Acta A Mol. Biomol. Spectrosc.* 278:121337
97. Sitarz K, Czamara K, Bialecka J, Klimek M, Szostek S, Kaczor A. 2021. Dual switch in lipid metabolism in cervical epithelial cells during dysplasia development observed using Raman microscopy and molecular methods. *Cancers* 13(9):1997
98. Pliss A, Kuzmin AN, Prasad PN, Mahajan SD. 2022. Mitochondrial dysfunction: a prelude to neuropathogenesis of SARS-CoV-2. *ACS Chem. Neurosci.* 13(3):308–12
99. Notarstefano V, Pisani M, Bramucci M, Quassinti L, Maggi F, et al. 2022. A vibrational in vitro approach to evaluate the potential of monoolein nanoparticles as isofuranodiene carrier in MDA-MB 231 breast cancer cell line: new insights from infrared and Raman microspectroscopies. *Spectrochim. Acta A Mol. Biomol. Spectrosc.* 269:120735
100. Bakar J, Michael-Jubeli R, Tfaili S, Assi A, Baillet-Guffroy A, Tfayli A. 2021. Biomolecular modifications during keratinocyte differentiation: Raman spectroscopy and chromatographic techniques. *Analyst* 146(9):2965–73
101. Wenzel T, Carvajal Berrio DA, Reisenauer C, Layland S, Koch A, et al. 2020. Trans-mucosal efficacy of non-thermal plasma treatment on cervical cancer tissue and human cervix uteri by a next generation electrosurgical argon plasma device. *Cancers* 12(2):267
102. Bik E, Orleanska J, Mateuszuk L, Baranska M, Majzner K, Chlopicki S. 2022. Raman and fluorescence imaging of phospholipidosis induced by cationic amphiphilic drugs in endothelial cells. *Biochim. Biophys. Acta Mol. Cell Res.* 1869(3):119186
103. Pacia MZ, Chorazy N, Sternak M, Fels B, Pacia M, et al. 2022. Rac1 regulates lipid droplets formation, nanomechanical, and nanostructural changes induced by TNF in vascular endothelium in the isolated murine aorta. *Cell. Mol. Life Sci.* 79(6):317
104. Lin J, Graziotto ME, Lay PA, New EJ. 2021. A bimodal fluorescence-Raman probe for cellular imaging. *Cells* 10(7):1699
105. Bader CA, Shandala T, Carter EA, Ivask A, Guinan T, et al. 2016. A molecular probe for the detection of polar lipids in live cells. *PLOS ONE* 11(8):e0161557
106. Chen Z, Paley DW, Wei L, Weisman AL, Friesner RA, et al. 2014. Multicolor live-cell chemical imaging by isotopically edited alkyne vibrational palette. *J. Am. Chem. Soc.* 136(22):8027–33
107. Gala de Pablo J, Chisholm DR, Ambler CA, Peyman SA, Whiting A, Evans SD. 2020. Detection and time-tracking activation of a photosensitiser on live single colorectal cancer cells using Raman spectroscopy. *Analyst* 145(17):5878–88
108. Watson MD, Lee JC. 2023. Genetically encoded aryl alkyne for Raman spectral imaging of intracellular α-synuclein fibrils. *J. Mol. Biol.* 435(1):167716. **https://doi.org/10.1016/j.jmb.2022.167716**
109. Yamakoshi H, Dodo K, Palonpon A, Ando J, Fujita K, et al. 2012. Alkyne-tag Raman imaging for visualization of mobile small molecules in live cells. *J. Am. Chem. Soc.* 134(51):20681–89
110. Samuel AZ, Miyaoka R, Ando M, Gaebler A, Thiele C, Takeyama H. 2020. Molecular profiling of lipid droplets inside HuH7 cells with Raman micro-spectroscopy. *Commun. Biol.* 3(1):372
111. Matuszyk E, Adamczyk A, Radwan B, Pieczara A, Szcześniak P, et al. 2021. Multiplex Raman imaging of organelles in endothelial cells. *Spectrochim. Acta A Mol. Biomol. Spectrosc.* 255:119658
112. Hekmatara M, Heidari Baladehi M, Ji Y, Xu J. 2021. D_2O-probed Raman microspectroscopy distinguishes the metabolic dynamics of macromolecules in organellar anticancer drug response. *Anal. Chem.* 93(4):2125–34
113. Matthäus C, Krafft C, Dietzek B, Brehm BR, Lorkowski S, Popp J. 2012. Noninvasive imaging of intracellular lipid metabolism in macrophages by Raman microscopy in combination with stable isotopic labeling. *Anal. Chem.* 84(20):8549–56
114. Stiebing C, Schmölz L, Wallert M, Matthäus C, Lorkowski S, Popp J. 2017. Raman imaging of macrophages incubated with triglyceride-enriched oxLDL visualizes translocation of lipids between endocytic vesicles and lipid droplets. *J. Lipid Res.* 58(5):876–83
115. Stiebing C, Matthäus C, Krafft C, Keller AA, Weber K, et al. 2014. Complexity of fatty acid distribution inside human macrophages on single cell level using Raman micro-spectroscopy. *Anal. Bioanal. Chem.* 406(27):7037–46

116. Ranneva SV, Okotrub KA, Amstislavsky SY, Surovtsev NV. 2020. Deuterated stearic acid uptake and accumulation in lipid droplets of cat oocytes. *Arch. Biochem. Biophys.* 692:108532
117. Egoshi S, Dodo K, Ohgane K, Sodeoka M. 2021. Deuteration of terminal alkynes realizes simultaneous live cell Raman imaging of similar alkyne-tagged biomolecules. *Org. Biomol. Chem.* 19(38):8232–36
118. Hill AH, Munger E, Francis AT, Manifold B, Fu D. 2019. Frequency modulation stimulated Raman scattering microscopy through polarization encoding. *J. Phys. Chem. B* 123(40):8397–404
119. Tipping WJ, Wilson LT, An C, Leventi AA, Wark AW, et al. 2022. Stimulated Raman scattering microscopy with spectral phasor analysis: applications in assessing drug-cell interactions. *Chem. Sci.* 13(12):3468–76
120. Hislop EW, Tipping WJ, Faulds K, Graham D. 2022. Label-free imaging of lipid droplets in prostate cells using stimulated Raman scattering microscopy and multivariate analysis. *Anal. Chem.* 94(25):8899–908
121. Stiebing C, Meyer T, Rimke I, Matthäus C, Schmitt M, et al. 2017. Real-time Raman and SRS imaging of living human macrophages reveals cell-to-cell heterogeneity and dynamics of lipid uptake. *J. Biophoton* 10(9):1217–26
122. Du J, Su Y, Qian C, Yuan D, Miao K, et al. 2020. Raman-guided subcellular pharmaco-metabolomics for metastatic melanoma cells. *Nat. Commun.* 11(1):4830
123. Oh S, Lee C, Yang W, Li A, Mukherjee A, et al. 2022. Protein and lipid mass concentration measurement in tissues by stimulated Raman scattering microscopy. *PNAS* 119(17):e2117938119
124. Ranjan R, Ferrara MA, Filograna A, Valente C, Sirleto L. 2019. Femtosecond stimulated Raman microscopy: home-built realization and a case study of biological imaging. *J. Inst.* 14:P09008
125. Li J, Condello S, Thomes-Pepin J, Ma X, Xia Y, et al. 2017. Lipid desaturation is a metabolic marker and therapeutic target of ovarian cancer stem cells. *Cell Stem Cell* 20(3):303–14.e5
126. Shi L, Klimas A, Gallagher B, Cheng Z, Fu F, et al. 2022. Super-resolution vibrational imaging using expansion stimulated Raman scattering microscopy. *Adv. Sci.* 9(20):2200315
127. Fung AA, Hoang K, Zha H, Chen D, Zhang W, Shi L. 2022. Imaging sub-cellular methionine and insulin interplay in triple negative breast cancer lipid droplet metabolism. *Front. Oncol.* 12:858017
128. Adams WR, Gautam R, Locke A, Masson LE, Borrachero-Conejo AI, et al. 2022. Visualizing the lipid dynamics role in infrared neural stimulation using stimulated Raman scattering. *Biophys. J.* 121(8):1525–40
129. Hong S, Chen T, Zhu Y, Li A, Huang Y, Chen X. 2014. Live-cell stimulated Raman scattering imaging of alkyne-tagged biomolecules. *Angew. Chem. Int. Ed.* 53(23):5827–31
130. Du J, Wei L. 2022. Multicolor photoactivatable Raman probes for subcellular imaging and tracking by cyclopropenone caging. *J. Am. Chem. Soc.* 144(2):777–86
131. Vukosavljevic B, Hittinger M, Hachmeister H, Pilger C, Murgia X, et al. 2019. Vibrational spectroscopic imaging and live cell video microscopy for studying differentiation of primary human alveolar epithelial cells. *J. Biophoton.* 12:e201800052
132. Zhang C, Boppart SA. 2020. Dynamic signatures of lipid droplets as new markers to quantify cellular metabolic changes. *Anal. Chem.* 92(24):15943–52
133. Levchenko SM, Kuzmin AN, Pliss A, Ohulchanskyy TY, Prasad PN, Qu J. 2019. Cellular transformations in near-infrared light-induced apoptosis in cancer cells revealed by label-free CARS imaging. *J. Biophoton.* 12:e201900179
134. Levchenko SM, Peng X, Liu L, Qu J. 2019. The impact of cell fixation on coherent anti-stokes Raman scattering signal intensity in neuronal and glial cell lines. *J. Biophoton.* 12:e201800203
135. Guerenne-Del Ben T, Couderc V, Duponchel L, Sol V, Leproux P, Petit JM. 2020. Multiplex coherent anti-Stokes Raman scattering microspectroscopy detection of lipid droplets in cancer cells expressing TrkB. *Sci. Rep.* 10:16749
136. Mizuguchi T, Momotake A, Hishida M, Yasui M, Yamamoto Y, et al. 2020. Multimodal multiphoton imaging of the lipid bilayer by dye-based sum-frequency generation and coherent anti-Stokes Raman scattering. *Anal. Chem.* 92(8):5656–60
137. Takei Y, Hirai R, Fukuda A, Miyazaki S, Shimada R, et al. 2021. Visualization of intracellular lipid metabolism in brown adipocytes by time-lapse ultra-multiplex CARS microspectroscopy with an onstage incubator. *J. Chem. Phys.* 155(12):125102

138. Mukherjee P, Aksamitiene E, Alex A, Shi J, Bera K, et al. 2022. Differential uptake of antisense oligonucleotides in mouse hepatocytes and macrophages revealed by simultaneous two-photon excited fluorescence and coherent Raman imaging. *Nucleic Acid Ther.* 32(3):163–76
139. Matuszyk E, Sierka E, Rodewald M, Bae H, Meyer T, et al. 2020. Differential response of liver sinusoidal endothelial cells and hepatocytes to oleic and palmitic acid revealed by Raman and CARS imaging. *Biochim. Biophys. Acta Mol. Basis Dis.* 1866(6):165763
140. Borek-Dorosz A, Grosicki M, Dybas J, Matuszyk E, Rodewald M, et al. 2022. Identification of inflammatory markers in eosinophilic cells of the immune system: Fluorescence, Raman and CARS imaging can recognize markers but differently. *Cell. Mol. Life Sci.* 79(1):52
141. Xu D, Liang S, Xu L, Bourdakos KN, Johnson P, et al. 2021. Widely-tunable synchronisation-free picosecond laser source for multimodal CARS, SHG, and two-photon microscopy. *Biomed. Opt. Express* 12(2):1010–19
142. Di Napoli C, Pope I, Masia F, Langbein W, Watson P, Borri P. 2016. Quantitative spatiotemporal chemical profiling of individual lipid droplets by hyperspectral CARS microscopy in living human adipose-derived stem cells. *Anal. Chem.* 88(7):3677–85
143. Camp CH Jr., Lee YJ, Heddleston JM, Hartshorn CM, Walker ARH, et al. 2014. High-speed coherent Raman fingerprint imaging of biological tissues. *Nat. Photon.* 8(8):627–34
144. Lakowicz JR. 2007. *Principles of Fluorescence Spectroscopy*. New York: Springer US. 3rd ed.
145. de la Rosa Rodriguez MA, Deng L, Gemmink A, van Weeghel M, Aoun ML, et al. 2021. Hypoxia-inducible lipid droplet-associated induces DGAT1 and promotes lipid storage in hepatocytes. *Mol. Metab.* 47:101168
146. Liu C, Zhang D, Ye S, Chen T, Liu R. 2022. D-π-A structure fluorophore: NIR emission, response to viscosity, detection cyanide and bioimaging of lipid droplets. *Spectrochim. Acta A Mol. Biomol. Spectrosc.* 267:120593
147. Niu J, Liu Y, Wang W, Lin W. 2019. Novel two-photon fluorescent probe with high fluorescence quantum yields for tracking lipid droplets in biological systems. *Spectrochim. Acta A Mol. Biomol. Spectrosc.* 216:35–44
148. Ramosaj M, Madsen S, Maillard V, Scandella V, Sudria-Lopez D, et al. 2021. Lipid droplet availability affects neural stem/progenitor cell metabolism and proliferation. *Nat. Commun.* 12:7362
149. Danylchuk DI, Jouard PH, Klymchenko AS. 2021. Targeted solvatochromic fluorescent probes for imaging lipid order in organelles under oxidative and mechanical stress. *J. Am. Chem. Soc.* 143(2):912–24
150. Wang J, Fang N, Xiong J, Du Y, Cao Y, Ji WK. 2021. An ESCRT-dependent step in fatty acid transfer from lipid droplets to mitochondria through VPS13D–TSG101 interactions. *Nat. Commun.* 12:1252
151. Lorent JH, Levental KR, Ganesan L, Rivera-Longsworth G, Sezgin E, et al. 2020. Plasma membranes are asymmetric in lipid unsaturation, packing and protein shape. *Nat. Chem. Biol.* 16(6):644–52
152. Lee HW, Lee IJ, Lee SJ, Kim YR, Kim HM. 2022. Highly sensitive two-photon lipid droplet tracker for in vivo screening of drug induced liver injury. *ACS Sens.* 7(4):1027–35
153. Xue H, Ge E, Ge W, Li J, Tian M. 2022. Single fluorescent probe for zero-crosstalk discrimination of lipid droplets and the endoplasmic reticulum based on reversible cyclization reaction. *Anal. Chem.* 94(25):9158–65
154. Wu CJ, Li XY, Zhu T, Zhao M, Song Z, et al. 2022. Exploiting the twisted intramolecular charge transfer effect to construct a wash-free solvatochromic fluorescent lipid droplet probe for fatty liver disease diagnosis. *Anal. Chem.* 94(9):3881–87
155. Lai C, Zhao Y, Liang Y, Zou X, Lin W. 2022. BF_2 group chelated AIE fluorescent probe for polarity mapping of lipid droplets in cells and in vivo. *Spectrochim. Acta A Mol. Biomol. Spectrosc.* 268:120637
156. Jung Y, Jin JH, Kim Y, Oh JH, Moon H, et al. 2022. Development of a fluorescent nanoprobe based on an amphiphilic single-benzene-based fluorophore for lipid droplet detection and its practical applications. *Org. Biomol. Chem.* 20(27):5423–33
157. Li X, Yang Z, Bian J, Fu M, Zhang Y, et al. 2022. Fluorescent probes based on multifunctional encapsulated perylene diimide dyes for imaging of lipid droplets in live cells. *Analyst* 147(7):1410–16
158. Öberg E, Appelqvist H, Nilsson KPR. 2017. Non-fused phospholes as fluorescent probes for imaging of lipid droplets in living cells. *Front. Chem.* 5:28

159. Huang B, Bates M, Zhuang X. 2009. Super-resolution fluorescence microscopy. *Annu. Rev. Biochem.* 78:993–1016
160. Yin J, Peng M, Lin W. 2019. Two-photon fluorescence imaging of lipid drops polarity toward cancer diagnosis in living cells and tissue. *Sens. Actuators B Chem.* 288:251–58
161. Kreder R, Pyrshev KA, Darwich Z, Kucherak OA, Mély Y, Klymchenko AS. 2015. Solvatochromic Nile Red probes with FRET quencher reveal lipid order heterogeneity in living and apoptotic cells. *ACS Chem. Biol.* 10(6):1435–42
162. Yamaguchi E, Wang C, Fukazawa A, Taki M, Sato Y, et al. 2015. Environment-sensitive fluorescent probe: a benzophosphole oxide with an electron-donating substituent. *Angew. Chem. Int. Ed.* 54(15):4539–43
163. Owen DM, Williamson DJ, Magenau A, Gaus K. 2012. Sub-resolution lipid domains exist in the plasma membrane and regulate protein diffusion and distribution. *Nat. Commun.* 3(1):1256
164. Sohn M, Toth DJ, Balla T. 2019. Monitoring non-vesicular transport of phosphatidylserine and phosphatidylinositol 4-phosphate in intact cells by BRET analysis. In *Intracellular Lipid Transport: Methods and Protocols*, ed. G Drin, pp. 13–22. New York: Springer
165. Tóth JT, Gulyás G, Hunyady L, Várnai P. 2019. Development of nonspecific BRET-based biosensors to monitor plasma membrane inositol lipids in living cells. In *Intracellular Lipid Transport: Methods and Protocols*, ed. G Drin, pp. 23–34. New York: Springer
166. Wilhelm LP, Voilquin L, Kobayashi T, Tomasetto C, Alpy F. 2019. Intracellular and plasma membrane cholesterol labeling and quantification using filipin and GFP-D4. In *Intracellular Lipid Transport: Methods and Protocols*, ed. G Drin, pp. 137–52. New York: Springer
167. Chandra A, Datta A. 2022. A peptide-based fluorescent sensor for anionic phospholipids. *ACS Omega* 7(12):10347–54
168. Moser von Filseck J, Čopič A, Delfosse V, Vanni S, Jackson CL, et al. 2015. Phosphatidylserine transport by ORP/Osh proteins is driven by phosphatidylinositol 4-phosphate. *Science* 349(6246):432–36
169. Chung J, Torta F, Masai K, Lucast L, Czapla H, et al. 2015. PI4P/phosphatidylserine countertransport at ORP5- and ORP8-mediated ER-plasma membrane contacts. *Science* 349(6246):428–32
170. Sohn M, Korzeniowski M, Zewe JP, Wills RC, Hammond GRV, et al. 2018. PI(4,5)P_2 controls plasma membrane PI4P and PS levels via ORP5/8 recruitment to ER-PM contact sites. *J. Cell Biol.* 217(5):1797–813
171. Capasso S, D'Angelo G. 2019. Imaging lipid metabolism at the Golgi complex. In *Intracellular Lipid Transport: Methods and Protocols*, ed. G Drin, pp. 47–56. New York: Springer
172. Hammond GRV, Schiavo G, Irvine RF. 2009. Immunocytochemical techniques reveal multiple, distinct cellular pools of PtdIns4*P* and PtdIns(4,5)P_2. *Biochem. J.* 422(1):23–35
173. Zhang J, Nie J, Sun H, Li J, Andersen JP, Shi Y. 2022. De novo labeling and trafficking of individual lipid species in live cells. *Mol. Metab.* 61:101511
174. Feng S, Harayama T, Montessuit S, David FP, Winssinger N, et al. 2018. Mitochondria-specific photoactivation to monitor local sphingosine metabolism and function. *eLife* 7:e34555
175. Kinoshita M, Suzuki KGN, Matsumori N, Takada M, Ano H, et al. 2017. Raft-based sphingomyelin interactions revealed by new fluorescent sphingomyelin analogs. *J. Cell Biol.* 216(4):1183–204
176. Brameshuber M, Weghuber J, Ruprecht V, Gombos I, Horváth I, et al. 2010. Imaging of mobile long-lived nanoplatforms in the live cell plasma membrane. *J. Biol. Chem.* 285(53):41765–71
177. Haberkant P, Stein F, Höglinger D, Gerl MJ, Brügger B, et al. 2016. Bifunctional sphingosine for cell-based analysis of protein-sphingolipid interactions. *ACS Chem. Biol.* 11(1):222–30
178. Höglinger D, Nadler A, Haberkant P, Kirkpatrick J, Schifferer M, et al. 2017. Trifunctional lipid probes for comprehensive studies of single lipid species in living cells. *PNAS* 114(7):1566–71
179. Gaebler A, Penno A, Kuerschner L, Thiele C. 2016. A highly sensitive protocol for microscopy of alkyne lipids and fluorescently tagged or immunostained proteins. *J. Lipid Res.* 57(10):1934–47
180. Bumpus TW, Liang D, Baskin JM. 2020. IMPACT: Imaging phospholipase D activity with clickable alcohols via transphosphatidylation. In *Methods in Enzymology*, Vol. 641: *Chemical Tools for Imaging, Manipulating, and Tracking Biological Systems: Diverse Chemical, Optical and Bioorthogonal Methods*, ed. DM Chenoweth, pp. 75–94. Amsterdam: Elsevier

181. Liang D, Wu K, Tei R, Bumpus TW, Ye J, Baskin JM. 2019. A real-time, click chemistry imaging approach reveals stimulus-specific subcellular locations of phospholipase D activity. *PNAS* 116(31):15453–62
182. Bumpus TW, Baskin JM. 2017. Clickable substrate mimics enable imaging of phospholipase D activity. *ACS Cent. Sci.* 3(10):1070–77
183. Gaebler A, Milan R, Straub L, Hoelper D, Kuerschner L, Thiele C. 2013. Alkyne lipids as substrates for click chemistry-based in vitro enzymatic assays. *J. Lipid Res.* 54(8):2282–90
184. Thiele C, Papan C, Hoelper D, Kusserow K, Gaebler A, et al. 2012. Tracing fatty acid metabolism by click chemistry. *ACS Chem. Biol.* 7(12):2004–11
185. Petersen BV, Gallion L, Allbritton NL. 2020. Silicon photomultipliers as a low-cost fluorescence detector for capillary electrophoresis. *Anal. Chem.* 92(20):13683–87
186. Dickinson AJ, Hunsucker SA, Armistead PM, Allbritton NL. 2014. Single-cell sphingosine kinase activity measurements in primary leukemia. *Anal. Bioanal. Chem.* 406(27):7027–36
187. Proctor A, Sims CE, Allbritton NL. 2017. Chemical fixation to arrest phospholipid signaling for chemical cytometry. *J. Chromatogr. A* 1523:97–106
188. Essaka DC, Prendergast J, Keithley RB, Palcic MM, Hindsgaul O, et al. 2012. Metabolic cytometry: capillary electrophoresis with two-color fluorescence detection for the simultaneous study of two glycosphingolipid metabolic pathways in single primary neurons. *Anal. Chem.* 84(6):2799–804
189. Ciura K, Dziomba S, Nowakowska J, Markuszewski MJ. 2017. Thin layer chromatography in drug discovery process. *J. Chromatogr. A* 1520:9–22
190. Whitmore CD, Olsson U, Larsson EA, Hindsgaul O, Palcic MM, Dovichi NJ. 2007. Yoctomole analysis of ganglioside metabolism in PC12 cellular homogenates. *Electrophoresis* 28(17):3100–4
191. Dickinson AJ, Meyer M, Pawlak EA, Gomez S, Jaspers I, Allbritton NL. 2015. Analysis of sphingosine kinase activity in single natural killer cells from peripheral blood. *Integr. Biol.* 7(4):392–401
192. Keithley RB, Rosenthal AS, Essaka DC, Tanaka H, Yoshimura Y, et al. 2013. Capillary electrophoresis with three-color fluorescence detection for the analysis of glycosphingolipid metabolism. *Analyst* 138(1):164–70
193. Proctor A, Allbritton NL. 2019. "Fix and assay": separating in-cellulo sphingolipid reactions from analytical assay in time and space using an aldehyde-based fixative. *Analyst* 144(3):961–71
194. Boardman A, Chang T, Folch A, Dovichi NJ. 2010. Indium–tin oxide coated microfabricated device for the injection of a single cell into a fused silica capillary for chemical cytometry. *Anal. Chem.* 82(23):9959–61
195. Wang Y, Yao M, Sims CE, Allbritton NL. 2022. Monolithic silica microbands enable thin-layer chromatography analysis of single cells. *Anal. Chem.* 94(39):13489–97